Science of the Total Environment 661 (2019) 575–597

Contents lists available at ScienceDirect

Science of the Total Environment

journal homepage: www.elsevier.com/locate/scitotenv

Groundwater hydrodynamics of an Eastern Africa coastal aquifer, including La Niña 2016–17 drought

Núria Ferrer [a,b,*], Albert Folch [a,b], Mike Lane [c], Daniel Olago [d], Julius Odida [d], Emilio Custodio [a,b,e]

[a] Department of Civil and Environmental Engineering, Universitat Politècnica de Catalunya, Jordi Girona 1-3, 08034 Barcelona, Spain
[b] Associated Unit: Hydrogeology Group (UPC-CSIC), Barcelona, Spain
[c] Rural Focus Ltd, Kenya
[d] Department of Geology, University of Nairobi, Kenya
[e] Royal Academy of Sciences of Spain, Spain

HIGHLIGHTS

- An East African costal aquifer was characterized before and during La Niña 2016/17.
- The recharge was reduced 69% compared to average annual rainfall.
- Lower recharge during first and nil recharge during the second wet season
- No important groundwater quality changes observed inland
- Increase of seawater intrusion even during the wet season

GRAPHICAL ABSTRACT

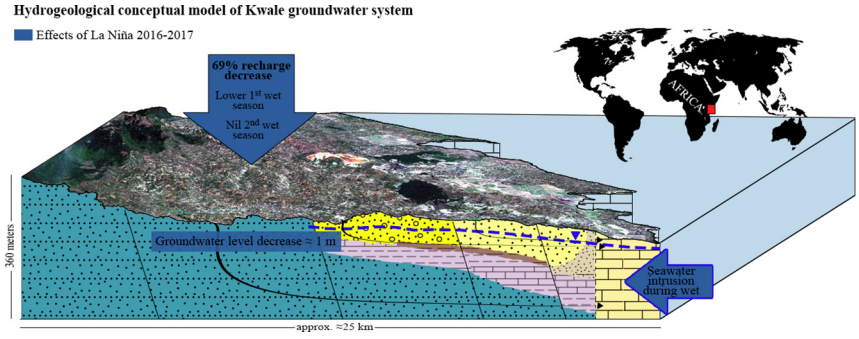

ARTICLE INFO

Article history:
Received 22 October 2018
Received in revised form 15 January 2019
Accepted 15 January 2019
Available online 16 January 2019

Editor: José Virgílio Cruz

Keywords:
Aquifer
Recharge
Saline intrusion
Hydrochemistry
Isotopes
Kenya

ABSTRACT

In 2016–17 much of East Africa was affected by a severe drought which has been attributed to Indian Ocean Dipole and El Niño Southern Oscillation conditions. Extreme events such as this have immediate and knock-on effects on water availability for household, agricultural and industrial use. Groundwater resources can provide a buffer in times of drought, but may themselves be stressed by reduced recharge and increased usage, posing significant challenges to groundwater resource management. In the context of East Africa, groundwater management is also hampered by a lack of information on aquifer characteristics. With the aim of addressing this knowledge gap, this study shows the hydrogeological behaviour before and during La Niña 2016/17 drought in southern coastal Kenya on a groundwater system which sits within a geological structure which is representative of an important portion of the East African coast. Diverse hydrochemical and isotopic campaigns, as well as groundwater head variation measurements, were carried out to study the groundwater hydrodynamics and thus characterize the aquifer system under climatic conditions before and during the La Niña event. This information is complemented with an estimation of changes in local recharge since 2012 using local data sets. The main consequence of the drought was a 69% reduction of recharge compared to an average climatic year. There was reduced recharge during the first rainy season (April–June) and no recharge during the second wet season (October–December). There was a concurrent increase in seawater intrusion even during the wet season.

* Corresponding author at: Department of Civil and Environmental Engineering, Universitat Politècnica de Catalunya, Jordi Girona 1-3, 08034 Barcelona, Spain.
E-mail address: nuria.ferrer.ramos@upc.edu (N. Ferrer).

https://doi.org/10.1016/j.scitotenv.2019.01.198
0048-9697/

1. Introduction

El Niño Southern Oscillation (ENSO) is a quasi-periodic invasion of warm sea surface waters into the central and eastern tropical Pacific Ocean, returning at least once in a ten-year period (Baudoin et al., 2017). Studies have shown correlations between ENSO conditions and monthly and seasonal rainfall patterns over East Africa (Mutemi, 2003). Oscillations in sea-surface temperatures in the Indian Ocean (known as the Indian Ocean Dipole, IOD) have also been shown to influence rainfall in the region (Behera et al., 2005; Ogwang et al., 2015). ENSO and IOD conditions triggered a severe drought in East Africa in 2016–17 (Uhe et al., 2018, 2017). The most affected areas include most of Somalia, south-eastern Ethiopia, north-eastern and coastal Kenya, and northern Uganda. Somalia and parts of Kenya faced severe famine. In South Sudan and Somalia, drought conditions made it harder to cultivate land and hampered humanitarian access, and in consequence, the drought led to the displacement of millions of people. In parts of Somalia and coastal Kenya, 70% to 100% crop failure was registered (Mpelasoka et al., 2017).

In Kenya, the first signals of an impending drought were experienced in October–December 2016 (Uhe et al., 2017). Kenya usually receives the majority of its rainfall during two periods: the 'long rains' during March, April and May (MAM) and the 'short rains' during October, November and December (OND) (Uhe et al., 2017). In 2016, the International Federation of Red Cross and the Red Crescent Societies (IFRC) noted that the south-eastern coast and north-western parts of Kenya received poor OND short rains, leading to an extension of the dry lean season that usually lasts from August to October. The south-east area had also suffered from poor MAM rains, intensifying the drought episode. The most affected Kenyan counties classified as "alarm stage" by the National Drought Management Authority were Turkana and Marsabit on the north-west and Kwale, Kilifi, Mombasa and Lamu on the south-east coast. The IFRC noted that the last drought reduced agricultural production and grazing lands for pastoralist communities and that the failed rains lead to decreased power and water supply to some of Kenya's communities (Uhe et al., 2017).

Due to the higher resilience of groundwater availability to droughts compared with surface water, groundwater resources are of particular importance during dry periods. However, aquifer water budgets and groundwater hydrodynamics are also affected by reduced rainfall. For this reason, it is important to characterize aquifer systems and understand their limitations in the face of future drought episodes (MacDonald et al., 2009). There are many African aquifer systems that have not yet been fully characterized, despite the importance of groundwater for growth and development (Comte et al., 2016). Poorly understood groundwater resources could be being used below their actual capacity, or be at risk of over-exploitation. Indeed, at a continental scale, 5 of the 8 largest world aquifer systems considered as over-exploited are located in Africa (Richey et al., 2015a, 2015b). Further research is required to underpin sustainable use and development of Africa's groundwater resources.

From a global comparison of scenario-based projections of population growth in low-elevation coastal zones, African coastal regions appear set to experience the highest rates of population growth and urbanization in the coming decades (Neumann et al., 2015), underlining the importance of groundwater resource management to meet population needs. Groundwater availability along the African coast was briefly reported in Steyl and Dennis (2010) but only some of the most populated areas have been studied in more detail. The South-east Tanzania Quaternary aquifer, which is the main water resource for the populated city of Dar es Salaam and its adjacent suburbs where around 80% of Tanzanian industry is located (Mtoni et al., 2013; Sappa et al., 2015; Van Camp et al., 2013), and the recently discovered regional Neogene aquifer (SE of Dar es Salaam) (Bakari et al., 2012), were studied in recent years. Of the Sub-Saharan African countries, South Africa has also had a number of hydrogeological investigations to define the country's aquifers (Day, 1993; Demlie and Titus, 2015; Kelbe et al., 2016; Ndlovu and Demlie, 2016). In Sub-Saharan Africa's low-income countries or regions, there have been very few additional studies. In Kenya, for example, coastal aquifers have been described by defining the current state of seawater intrusion (Obura, 2001; Okello et al., 2015) and Ezekiel et al. (2016) provide an assessment of the vulnerability of the Mombasa coastal aquifer. In many areas of Africa, the lack of groundwater monitoring and/or geological studies makes adequate aquifer characterization difficult.

ENSO and IOD-related droughts must be considered as one of several threats to groundwater availability in coastal Africa in coming decades. In order to improve water resources management and planning, this study provides evidence of the effect of the drought which began in 2016 on the groundwater systems of the East African coast. The groundwater system located in Kwale County (Kenya) has a geological structure that is representative of an important portion of the East Coast of Africa (Rais-Assa, 1988) and was thus chosen as a paradigmatic example for study aimed at understanding the impact of severe drought on a coastal aquifer system in a rural area of relatively low population. This contrasts the recent studies carried out in Dar es Salaam and South Africa, which focused on aquifers in highly populated urbanized zones.

This paper has two specific objectives: 1) Define the hydrodynamics of the Kwale hydrogeological system, and 2) show the effects of the La Niña 2016/17 drought on the groundwater system.

This paper includes the results of a geophysical survey conducted to define the aquifer geometry forming the basis of the conceptual model. Local meteorological and soil data, hydrochemical field surveys and groundwater levels were used to describe aquifer recharge, groundwater flow direction, connectivity between aquifer layers, and prevalence of pollution. The effects of La Niña on the hydrogeological system were assessed by comparing data from before and during the drought episode.

2. Study area

The study area is located in a rural area on the coastal plain of Kwale County, south of Mombasa and adjacent to northern Tanzania (Fig. 1). The county, which has one of the highest poverty rates in Kenya, has a population around 798,000 ("Commission on Revenue Allocation,", 2018), most of whom reside in rural areas (82%) (CWSB, 2013a; Foster and Hope, 2016), concentrated mainly along the coast. Only 65.8% of Kwale's population has access to improved water in households in 2009 and 48.6% to improved sanitation ("Commission on Revenue Allocation,", 2011).

The physiography of the region is divided into three units: The Coast Plain at an elevation generally below 30 m asl (above sea level); the Foot Plateau which has an elevation ranging from 60 to 135 m asl, and the Coastal Range formed by the Shimba Hills with elevation ranging generally from 150 to 455 m asl (Buckley, 1981) (Fig. 2). The area slopes toward the sea. The area beyond the Shimba Hills drains to a river basin flowing south-east.

In the coastal area, the precipitation range is between 900 and 1500 mm/year and the average temperature is about 26.5 °C. Inland, west of the Shimba Hills, the precipitation ranges from 500 to 600 mm/year and the temperature varies from 25 to 26.6 °C (CWSB, 2013b).

As already said, the area is characterized by a bimodal rainfall pattern and experiences considerable climate variability (Mumma et al., 2011). In Kenya, the "long rains" generally fall from March to May (MAM) but in the study area in recent years the long rains have been delayed and fall from April to June, while the "short rains" occur between October and December (CWSB, 2013a, 2013b).

From May 2016 to early 2017 the study area experienced unusually dry conditions. Local weather data suggest that this period represents the most extreme drought since 1974 in this area. The precipitation in the rain gauge at Kwale Agricultural Department Station (KMD

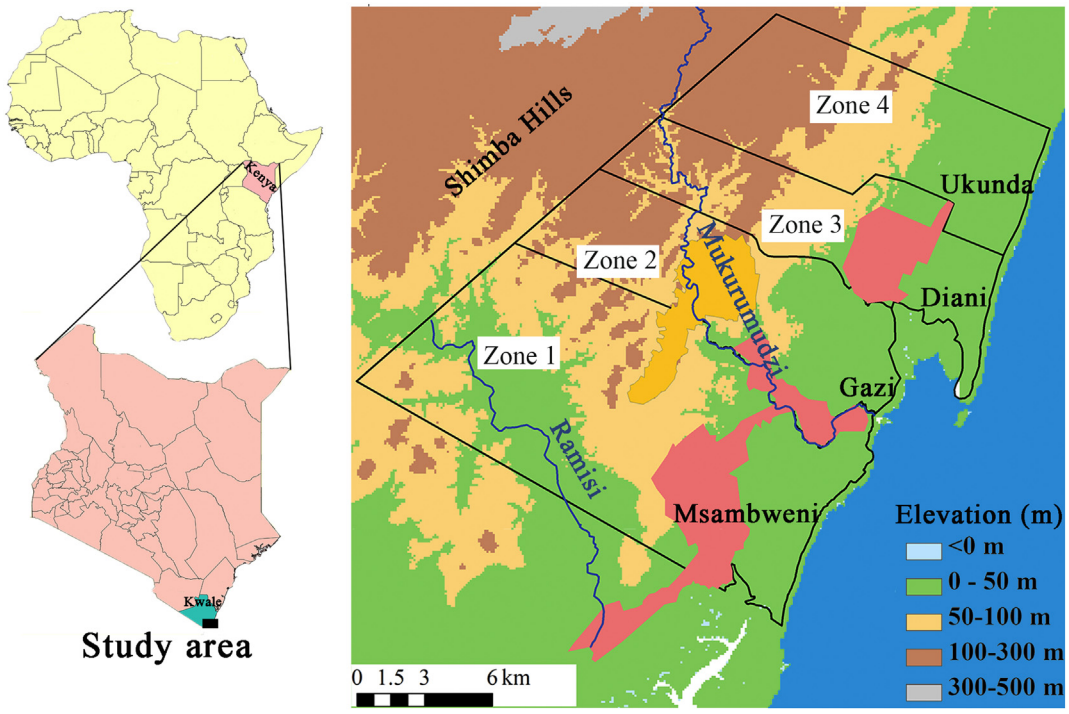

Fig. 1. Location of the study area in Kwale County (Kenya). The orange area is the Base Titanium mining site; the red area corresponds to the KISCOL sugar fields and the green areas are forests. The study area is divided into the four zones shown, which have been set to help the reader throughout this paper. (For interpretation of the references to color in this figure legend, the reader is referred to the web version of this article.)

9439001) in Kwale town in the north-west of the study area was 636 mm/year in 2016. Rainfall in the same station in 2013, 2014 and 2015 was 1286, 1604 and 1345 mm/year respectively. In recent years, from 2012 to 2017, the average rainfall depth is around 1145 mm. In 2013 (1286 mm) and 2017 (1265 mm) the rainfall was close to the average while in 2012 and 2016 were both well below the average, and 2014 and 2015 were well above. During 2016, some community wells dried up completely.

The population in the study area lives in small scattered communities and engages in extensive stockbreeding. The coastal areas host urban communities, including Ukunda, Msambweni and Diani. Population decreases inland away from the coast. Most of the local economy is based on small-scale agriculture, but there are two other major activities: industrial agriculture (sugar-producing company KISCOL) and mineral exploitation (mining company Base Titanium).

3. Geology

The main rocks in the area range from the Carboniferous to Plio-Pleistocene in age and overlie the metamorphic rocks of the Mozambiquan system (Caswell, 1953; Rais-Assa, 1988). Much of the geology to the east is covered by the Magarini and Kilindini sands. The oldest of these formations is the Taru Fm. (Upper Carboniferous to Middle Permian). The Maji ya Chumvi Fm. (Mid-Permian to Mid-Triassic) overlies conformably on top of the Taru Formation and comprises sandstones and Carboniferous shales, sandy shales with fossil fish fauna, and argillaceous sandstones that reflect a lacustrine deposition paleoenvironment (Rais-Assa, 1988) and a period of fluctuating climate (wet to dry) with possible evaporate deposits (Caswell, 1953). The Mariakani Fm. (Middle to Upper Triassic) covers conformably the Maji ya Chumvi Fm. (Rais-Assa, 1988).

The formations that outcrop in the study area are the Mazeras Fm. (Lower Jurassic to the start of Middle Jurassic), the Kambe Fm. (Start of Middle Jurassic to middle Upper Jurassic), and the Mtomkuu Fm. (from the Middle of the Upper Jurassic to the Cretaceous) (Rais-Assa, 1988) (Fig. 2). These are overlain, following a long hiatus, by Cenozoic rocks and unconsolidated materials that include the Magarini sands (Upper Pliocene) dunes, coral reefs (Lower to Middle Pleistocene), the lagoonal Kilindini sands (Upper Pleistocene) and younger mostly sandy deposits (Caswell, 1953; Rais-Assa, 1988). The Mazeras Fm. is divided into two, the Lower and Upper Mazeras (Rais-Assa, 1988). The Lower Mazeras has coarse sandstones with silicified wood horizons, while the Upper Mazeras (roughly constrained above the 272 m elevation contour line) comprises quartz-feldspathic sandstones and grits (Shimba grits) at the top (Cannon et al., 1981; Caswell, 1953; Rais-Assa, 1988). The Mazeras rocks have been estimated to attain a total thickness of at least 305 m (Caswell, 1953) and are ascribed to a deltaic to aeolian facies (Rais-Assa, 1988). The Kambe Fm., a marine facies, has conglomerates and limestones in the lower part and shales, sandstones and limestones in the upper parts (Rais-Assa, 1988), and sits above on a major angular erosional discordance that separates it from the Shimba grits (Caswell, 1953; Rais-Assa, 1988). The Mtomkuu Fm. rests upon a major angular unconformity with the Upper Kambe Fm., and has silty clays in the lower part and shales, sandstones and limestones in the upper part, representing a transgressive marine facies (Rais-Assa, 1988). These three formations and the overlying Cenozoic sediments constitute the medium to high potential aquifers in the study area.

Related geological and geophysical work that was undertaken as part of this project has revealed that there are two paleochannels in the study area, located in zone 1 and 4 (Fig. 2) (Olago D., Odida J. and Lane M., pers. comm.). They were formed by the erosion of Kambe Fm. and Mtomkuu Fm. during the last low sea stand and subsequent infilling by fluviatile sediments with very likely thin impermeable layers of e.g. fine consolidated fluvial sands, clays and indurated bioclastic sands. Clusters of high capacity boreholes lie within these paleochannels at Milalani (zone 1) and Kinondo (zone 4).

4. Methodology

In order to construct the conceptual model and characterize the hydrogeological system during the La Niña event in 2016, different surveys were carried out in the study area.

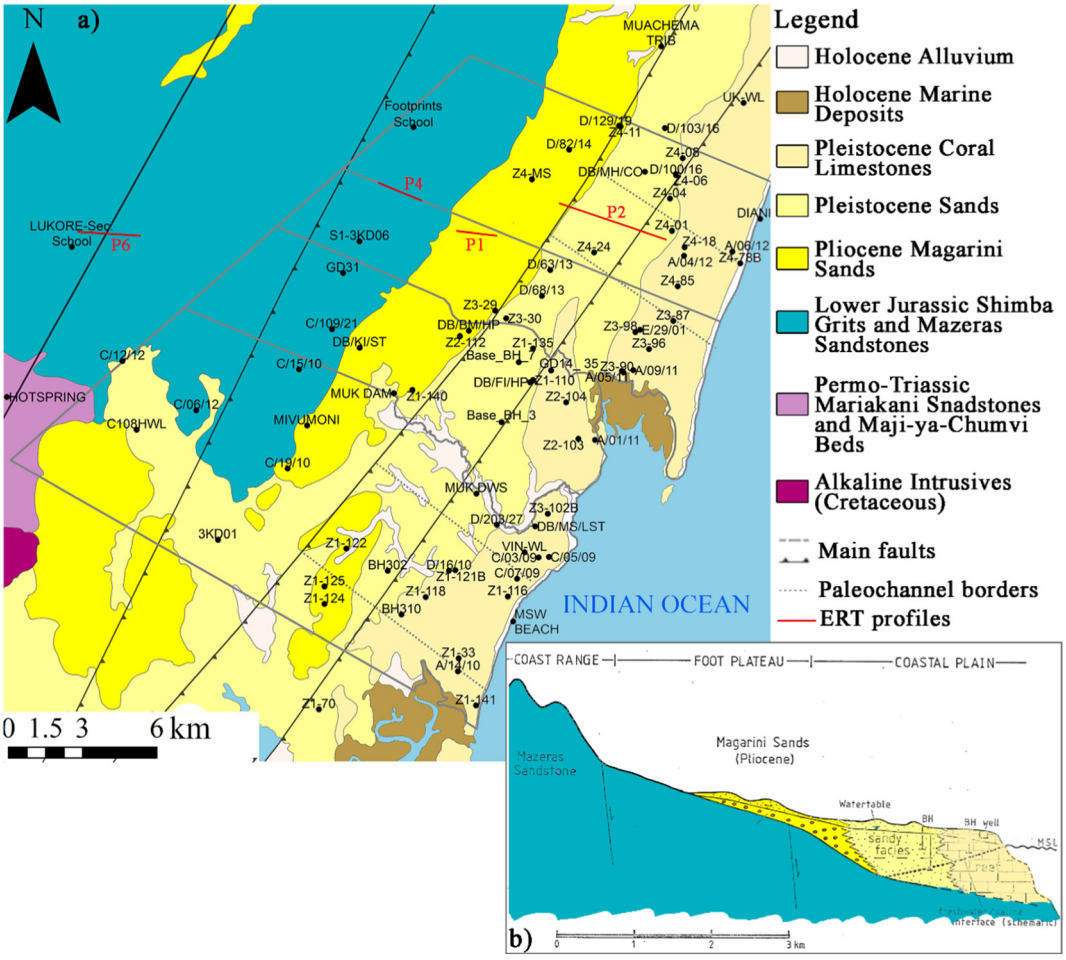

Fig. 2. a) Geological map with the main faults, the main paleochannels (grey dotted lines), the sampled points in June 2016 and in red the ERT profiles. Geologically surveyed by D.O. Olago, J. Odida, and M. Lane (2018), ©University of Nairobi. b) The idealized cross-section of the study area (modified from Buckley, 1981). (For interpretation of the references to color in this figure legend, the reader is referred to the web version of this article.)

Water samples were taken from wells and boreholes at different depths and in different geological formations to characterize all aquifer systems in the study area. Because of the complexity of the available sampling points, the efforts were focused on identifying distinct hydrogeological interactions and on providing a complete description of groundwater dynamics.

4.1. Geophysical surveys

An ERT (electro-resistivity tomography) study was conducted between December 2015 and June 2016 to define the aquifer geometry in the study area. This was supported by geological field studies. A 2-D electrical imaging/tomography survey equipment was used. The field set of the tomography system used in this research included an ABEM SAS 1000 Terrameter, LUND ES464 switchbox (an electronic switching unit), 4 multi-core cables each with 21 current take out points at constant spacing of 10 meters interval, battery, communications cables, electrode jumpers, electrodes, laptop, and data transfer cable. The profile length was 800 m, comprising four multi-core cables. Roll-along technique was used during data acquisition. After completing the sequence of measurements, the cable was moved past one end of the line by two cables. The investigated depth was 149 m bgl (below ground level). This set-up provides a 2-dimensional inversion of the resistivity measurements along a profile line. The data was acquired in E-W orientation and NNE-SSW orientation, parallel to the coastline. ERT data was analysed using the RES2DINV inversion software.

4.2. Recharge

In order to estimate the effect of La Niña drought on the seasonal and annual recharge patterns, groundwater recharge was estimated for the period 2012 to 2017 from the daily soil water budget. Groundwater recharge was calculated for the main land cover of the study area, with 65% of it defined as open: broadleaved deciduous trees with closed to open shrubs, based on Africover database (DiGregorio, 2002).

Rainfall data was obtained from Kwale Agricultural Department rainfall station manned by Kenya Meteorological Department (KMD) located in Kwale Town. The other meteorological parameters such as temperature, wind speed, evaporation and humidity were obtained from the SWAT Global Weather (Soil and Water Assessment Tool), NASA, Kenya Meteorological Department and TAMHO (Gathenya, Thomas, pers. com). ETP was calculated by Hargreaves equation (Hargreaves and Samani, 1982). The recharge rate was estimated based on the soil mass balance by considering soil composition, root deep and threshold runoff. Soil composition was obtained from Kensoter ver.2 database (Kempen, 2007). This database consists of a soil inventory, which includes the geographical distribution of the soil units, the percentage of clay, silt and sand characteristic of each soil type, and their specific TAWC (Total Available Water Content) value. The root depth of the land cover was obtained from the Food and Agricultural Organization (FAO) (www.fao.org). Finally, the threshold runoff was calculated for each land use by applying data from theoretical tables (Miller, 1994).

4.3. Background monitoring

An aquifer monitoring program was developed to measure groundwater level and physicochemical parameters: temperature, electrical conductivity (EC) and pH, from January 2014 until present. A total of 43 points in the Magarini sands, Kilindini sands and Pleistocene corals were monitored every two weeks (from 4 m bgl to 27 m bgl). The groundwater level was taken using a Heron level probe and the physicochemical parameters were measured using Eutech COND 6+ conductivity meter (EC25 and temperature) and Eutech pH 6+ pH/ORP meter (pH and Eh).

This data was complemented with information from Base Titanium's monitoring network composed of piezometers and community wells (from 5 m bgl to 107 m bgl) spread mainly around the mining site, starting in March 2007 (field water quality) and August 2011 (water level data).

4.4. Hydrochemical and isotopic sampling surveys

Sampling campaigns were carried out in the study area in March (end of dry season) and June (end of wet season) to enable assessment of hydrochemical conditions in different seasons of a wet year (2014) and in the La Niña-affected year (2016). During the field campaigns carried out in 2014, 32 and 34 wells/boreholes up to 30 m deep were sampled in the dry (March) and wet (June) season respectively. During the field survey of 2016, the number of sampling points was increased to 75 in March and to 80 in June, since more samples were needed to better define the groundwater system. This included an additional sampling of wells/boreholes in the Shimba Hills and a number of deep boreholes across the study area. The 2016 surveys also included surface water samples: 2 in Ramisi River (C108HWL and 3KD01), 3 in Mukurumudzi River (S1-3KD06, MUK DAM and MUK DWS) and 1 in Mwachema River (MWACHEMA TRIB) (Fig. 1). In 2016 water isotopes were also analysed in both field surveys.

Samples for hydrochemical and isotopic analysis were taken from wells used daily. For boreholes fitted with a handpump, it was ensured that at least three casing volumes of groundwater were removed before sampling. In the case of open wells, samples were taken using an electrical pump when the water column allowed. A bucket was used as a last option. The physicochemical parameters measured in situ during the 2016 sampling campaign were: temperature, pH, EC_{25} (electric conductivity at 25 °C), DO (dissolved oxygen) and Eh measured with a YSI Professional Plus multiparameter probe with a flow cell to avoid contact with the air. pH and EC_{25} measurements are automatically temperature compensated. In 2014 the field parameters were measured with a Eutech COND 6+ conductivity meter (EC_{25} and temperature) and Eutech pH 6+ pH/ORP meter (pH and Eh). The pH was periodically calibrated against pH 7.00 and 4.04 references before and during the field surveys. EC_{25} was periodically calibrated against a 1413 μS/cm reference solution before and during the field surveys. All probes were washed in distilled water before and after each measurement and the probes were kept with distilled water all time. In addition, in 2016, ammonium concentration (NH_4-N and NH_4^+) was measured in situ by a field colorimeter test with a color card comparator manufactured by Merck Millipore. Alkalinity concentration (carbonate, CO_3^{2-} and bicarbonate, HCO_3^-) was also measured in situ, after filtering the sample with 0.2 μm filters, by field titration using a digital titrator manufactured by Merck Millipore in the 2016 field surveys, and by field titrator manufactured by HACH in 2014 field surveys.

Samples for cation, anion and trace element analysis were filtered in the field with 0.2 μm GNWP (Millipore) nylon membrane in 15 mL polypropylene bottles, in 2016. In 2014, samples were filtered with 0.45 μm filters (Sartorius) and collected in 130 mL polypropylene bottles. One membrane was used for each sampled point. After filtering, the bottles for cation and trace elements samples were acidified with 70% pure HNO_3 to ensure that pH < 2. Water isotopes were collected in 2 mL special crystal chromatography tubes with their respective septum cup without headspace. Total Organic Carbon (TOC) was sampled with crystal bottles (previously sterilized in a muffle furnace), filled without headspace and acidified in the field with HCl 2 N. Water isotopes and TOC were analysed only in 2016 field surveys.

The samples were kept at 4 °C in a dark cool box during the field day and stored at 4 °C until they were analysed in the laboratory. The cations, trace metals and TOC collected in 2016 were analysed by the Institute of Environmental Assessment and Water Research (IDAEA) by ICP-AES, ICP-MS and by an infrared detector using the NPOC method (Shimatzu TOC-Vcsh) respectively. In the 2014 campaigns, cations were analysed by ICP-OES. Anions (campaigns in 2016) were processed by the Catalan Institute of Water Research (ICRA) using ionic chromatography. Bromide was analysed at the Grup de Tècniques de Separació (GTS) of the Autonomous University of Barcelona by ICP-MS. In 2014 field campaigns, the laboratory used a Water Analyser to measure anion concentrations. Water isotopes (δD and $\delta^{18}O$) were measured in the Centro de Hidrogeología de la Universidad de Málaga (CEHIUMA) using Picarro equipment. For δD and $\delta^{18}O$ the notation is expressed in terms of δ‰ relative to the international standard V-SMOW (Vienna Standard Mean Oceanic Water). The precision of the samples calculated from international and internal standards systematically interspersed in the analytical batches was ±0.3‰ for δD and ±0.05‰ for $\delta^{18}O$. The quality of the chemical analysis was checked by performing the ionic mass balance. The hydrochemical composition of samples with error >10% was not taken into account in the hydrochemical results.

5. Results

5.1. Aquifer structure based on geological and geophysical data

The profiles, from west to east, are in sequence 6, 4, 1 and 2 (Fig. 2). In Profile 6 the surface geology is weathered Mazeras Sandstones with some slightly weathered patches. At depth, there are no clearly defined lithological structures and this probably reflects the spatially and vertically heterogeneous nature of these deltaic and aeolian-derived, folded and compacted sediments, with occasional aquifers. The highly weathered fracture zone(s) in the sandstones are potential aquifers, with good water quality reported at Lukore Dispensary, Lukore Secondary and Mukanda sites. Profile 4 clearly shows two aquifer layers; a shallow (up to 30 m) unconfined aquifer with generally low resistivity reflecting lenses of saline water, and a deeper aquifer with higher resistivity (50–200 Ω m). Profile 4 sub-surface topography indicates that the rocks of the Mazeras, Kambe and Mtomkuu Fm. are folded, consistent with Rais-Assa's (1988) observations. While the Mazeras sandstone can easily be differentiated on the basis of its relatively high resistivity (>300 Ω m), the Kambe and Mtomkuu Fm. are geophysically indistinguishable, perhaps partly due to their relatively high water bearing capacity or their relatively small thickness. Profile 1 surficial geology consists of Magarini Sands with relatively flat topography. The geophysical results indicate possible potential aquifers between 20 m and 80 m bgl (Fig. 3).

Multiple rivers were observed traversing the area. Fresh (low resistivity, 30–100 Ω m) to saline (very low resistivity, <30 Ω m) unconfined groundwater is indicated, depending on the locality, up to depths of ca. 30 m. A major fracture zone trending NNE-SSW with a down throw to the east is inferred (fault 3 on Fig. 1), with a surface expression 380 m long. Profile 2 was 3000 m long. Its surface geology comprised Kilindini sands to the west and Pleistocene corals to the east. From the geophysical results, the tongue-shaped structure at the eastern end of the profile depicts a possible underground cavern from the dissolution of corals. There is a barrier that restricts movement of saline water further inland. In the subsurface and close to the present-day shoreline, corals can be inferred to a depth of about 100 m bgl.

Consequently, the outline of the hydrogeology of the area is fairly simple. The groundwater system comprises a shallow aquifer system

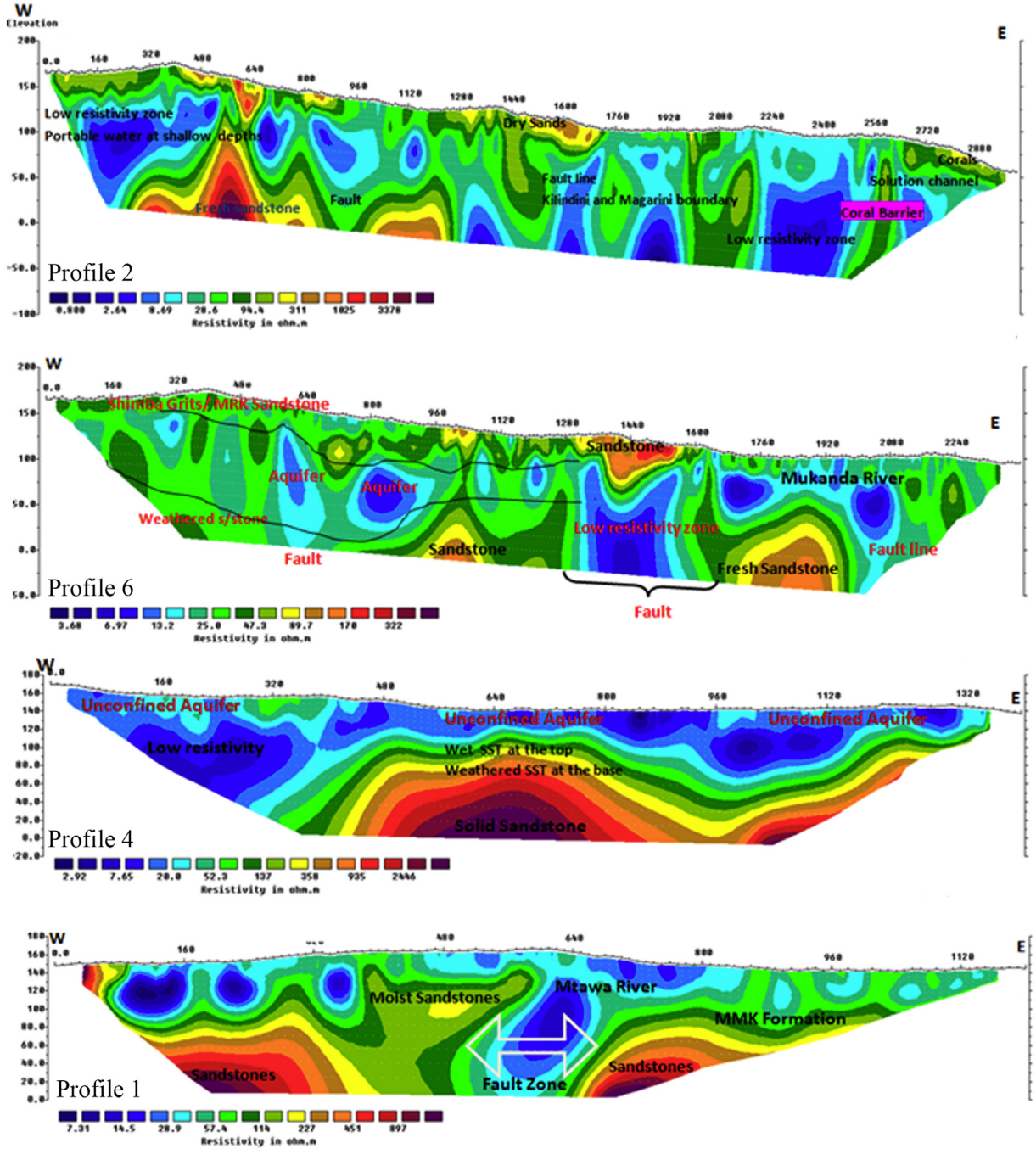

Fig. 3. Geophysical profiles located on the study area in Fig. 2.

recharged directly by rain infiltration, and a deeper aquifer that is recharged laterally from the Shimba Hills area acting as a mountain-front area.

5.2. Recharge

Groundwater recharge evolution according to the soil water balance is shown in Fig. 4. The recharge was calculated for the main land cover of the study area which cover the area of Shimba Hills. Therefore, the estimated recharge volume represents mainly the recharge in the upper parts of the study area. The recharge volume in the middle and southern area could differ a bit, since it depends on the land cover and soil properties. It should be interesting to estimate the recharge calculating the soil mass balance for each type of land cover combined with the diverse soil properties present in the area.

Despite the very short time series, only 5 years, there is significant variation over time. In 2014, the wettest year of the period, precipitation was 1591 mm while in 2016, during the drought event, precipitation was 636 mm, less than half of that and 13% less than total precipitation in the second driest year.

Groundwater recharge occurs mainly during the wet season. During the studied period (2012–2016), for 97% of period, no recharge was observed. It was estimated that unless accumulated rainfall in a given rain period is >104 mm, little or no recharge occurs. These observed thresholds reflect the requirement of prolonged rainfall events to generate recharge due to high rates of evapotranspiration and soil moisture deficit. Daily potential evapotranspiration is often higher than daily rainfall

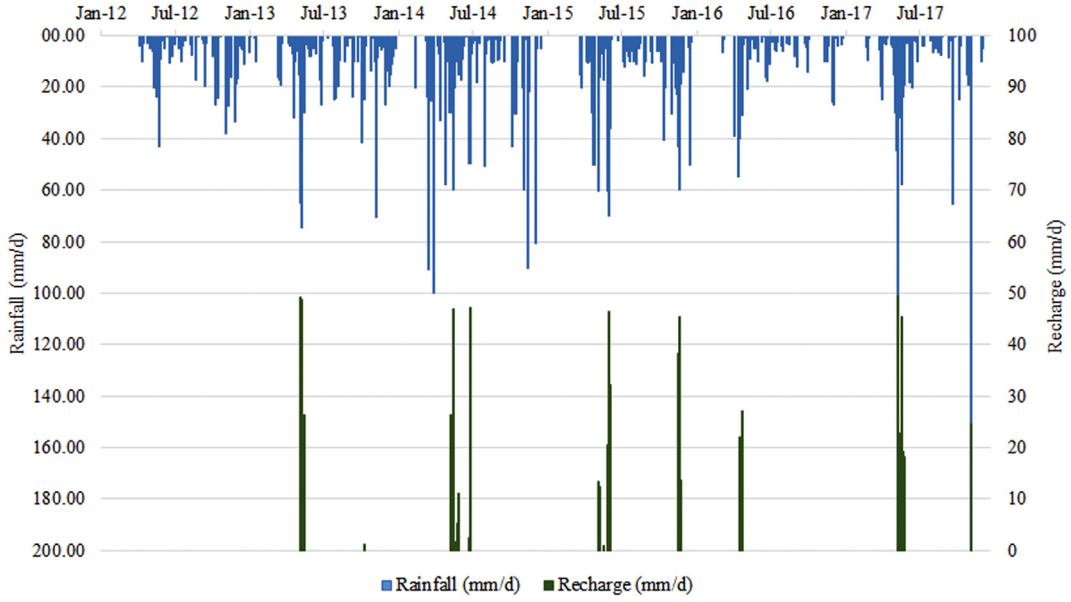

Fig. 4. Recharge rate based on daily soil mass balance vs. rainfall at Kwale Agricultural Department station (Kenya Meteorological Department) (mm/day); January 2012 to October 2017.

depth in the area. The relationship between rainfall and groundwater recharge is nonlinear. Seasonal rainfall depth is important, as is rainfall pattern across the seasons. This observation agrees with Taylor et al. (2012), which notes that intense seasonal rainfall associated with the El Niño Southern Oscillation and the Indian Ocean Dipole mode of climate variability contributes disproportionately to recharge. Indeed, infrequent recharge associated with heavy rainfall events is common in semiarid climates with retentive soils (Custodio et al., 1997).

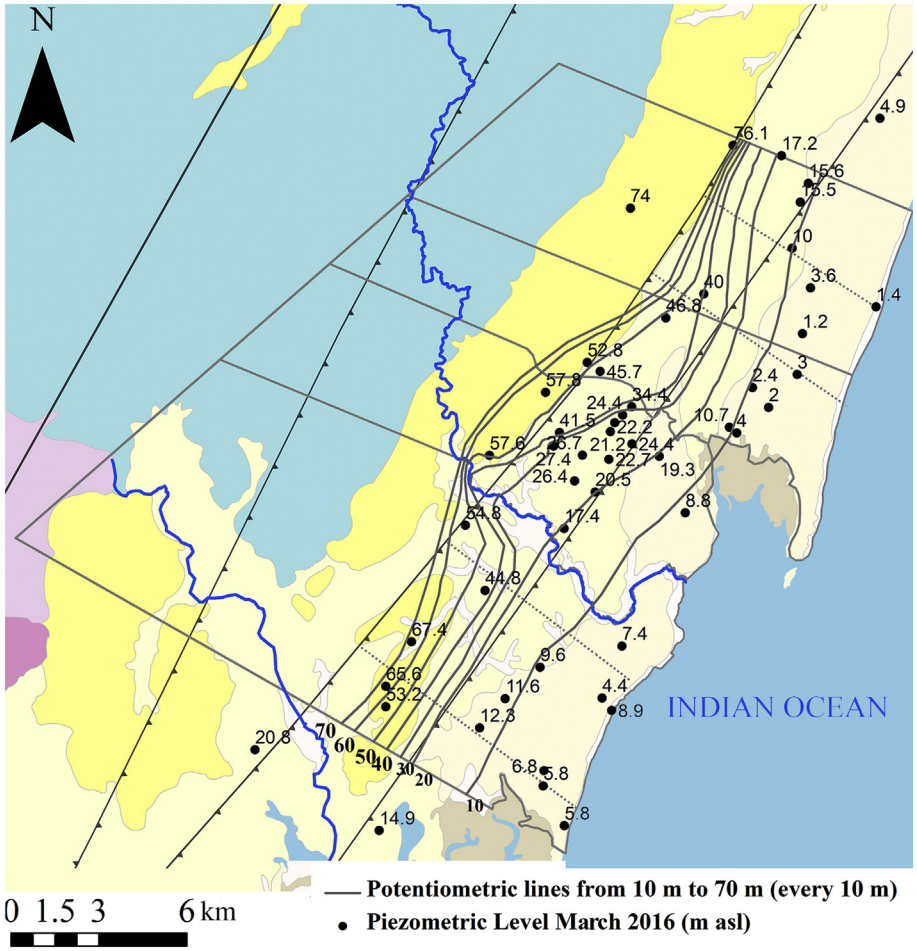

Fig. 5. Groundwater piezometric level contour map for the shallow aquifer in March 2016 after the field survey, relative to mean sea level. Potentiometric lines are represented every 10 m. The two measured wells located south study area present different hydrogeological behaviour, so they had not been included in the piezometric contour map.

During the wet year 2014, the main recharge periods are well differentiated: April to June (long rains) has the highest recharge with less recharge in October to December (short rains). During the La Niña event, groundwater recharge volume was reduced during both wet seasons. During the long rains period, there was a recharge peak due to rainfall events of over 145 mm/day in April 2016. However, as stated in Uhe et al. (2018, 2017), the OND short rainfall period was particularly badly hit by the La Niña event, and the results of the investigation done indicate no recharge during this period (Fig. 4).

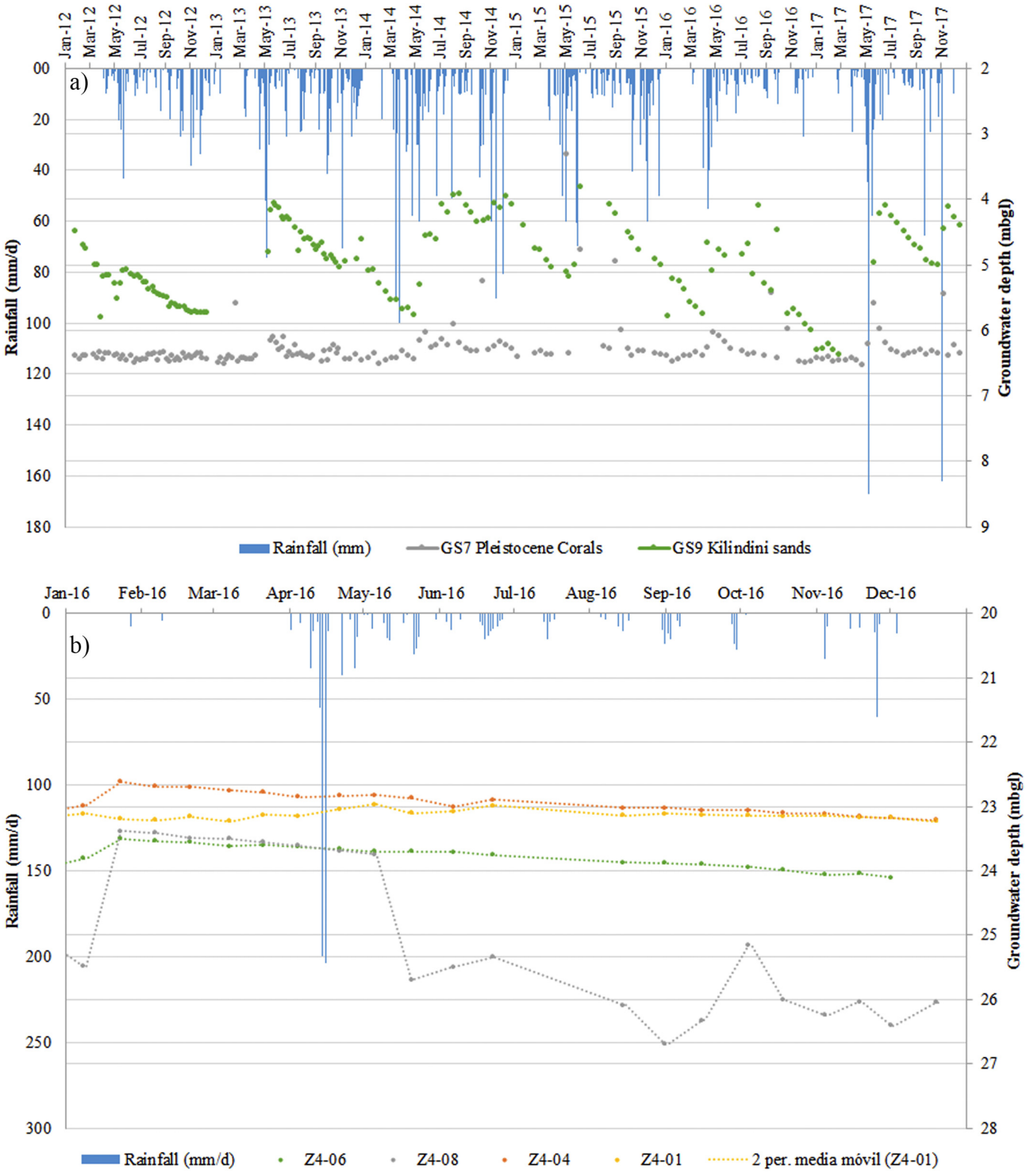

Fig. 6. a) Groundwater level over time in well located in the Kilindini sands (GS9) and in well located in the Pleistocene corals (GS7). Peaks are insinuated in the corals during some recharge events indicating the fast response of the aquifer to rains. They did not show up in other recharge events due to the low frequency of measurements. b) Groundwater level in 2016 in community wells located to the North of the study area in the Kilindini sands (see Fig. 1). Plots also show rainfall at Kwale Agricultural Department station (Kenya Meteorological Department) (mm/day).

5.3. Groundwater distribution and trends

Groundwater flow in the shallow aquifer is from the upper part of the study zone to the lowest zones at the coast, discharging along the littoral and offshore into the sea (Fig. 5). The majority of discharge from both aquifers is assumed to be submarine to the Indian Ocean. There are a number of brackish groundwater emergences in the tidal zone observed along Diani coast and Msambweni Beach. In the middle part of the study area, the shallow aquifer feeds the gaining Mukurumudzi River while the surface-groundwater interaction in the Ramisi river cannot be defined with available water level data.

The Kilindini sands constitute the main extension of the shallow aquifer in the study area. Most of the groundwater recharge in this geological formation occurs during intense rains or long rainy periods in April to June (Fig. 6a). The response of the water table to important rains is relatively fast, with peak water level occurring between 7 and 20 days after the main rainfall (Fig. 6a). Increasing groundwater level is accompanied by decreasing EC (Table 1).

The effect of La Niña 2016/2017 event on groundwater level variation in the Kilindini sands aquifer is shown in a well (GS9) located in this geological formation (Fig. 6a). During the low rainy periods, such as during La Niña, the descent of groundwater level continued until the next relevant rainfall event. 2012 was a very dry year with low OND rainfall, only slightly more than that in 2016. From January to December 2016, the groundwater level variation measured in wells located in this geological formation was between a maximum of 3.4 m and a minimum of 1.4 m (Table 1).

However, some wells located in the Kilindini formation in the north of the study area (points Z4-06, Z4-08, Z4-04 and Z4-01 in Fig. 1) show a different pattern in the response of groundwater level to rainfall (Table 1). These wells show lower increases in groundwater level after large rainfall events (Fig. 6b).

Rapid infiltration after rainfall events in the Pleistocene corals, attributed to high hydraulic diffusivity (T/S), causes recharge peaks in wells in this formation to dissipate rapidly (Fig. 6a grey dots). The same process explains the sharper response of groundwater levels to rainfall compared to that seen in the unconfined Kilindini sands (Table 1). These recharge peaks are to be expected due to karstification of the geological formation. The reaction is not observed after all the main rainfall events due to the low frequency of measurements (every 15 days).

The deep aquifer is exploited by some community wells, KISCOL and Base Titanium. Only Base Titanium has monitoring points not directly affected by dynamic groundwater levels due to abstraction. For this reason and because of the geological heterogeneity in the study area, the deep aquifer behaviour can be only described in the middle part of the study area. Groundwater level in deep boreholes also reacts to rainfall, as the shallow aquifer piezometers do, but there are somewhat longer lags between the start of recharge and the groundwater level maximum in the confined aquifer compared with the shallow aquifer; this time lag is 13–20 days (Table 2 Supplementary material).

Water level measurements from the Base Titanium shallow piezometers show a limited effect of pumping from the deep aquifer on shallow groundwater level. This limited/nil effect is attributed to a low permeability aquitard between the two aquifers, which was observed during the drilling of the Base Titanium boreholes. Groundwater level in the deep aquifer shows the influence of groundwater abstraction in this area, which started in 2014 (Fig. 7). The marked drawdown during the 2016 drought may have been enhanced by groundwater abstraction during the same period made by Base Titanium.

Table 1
Groundwater level range and EC range of some monitored points from 2016 to April 2017.

Point	Geology	Zone	Aquifer	Dates	EC range	EC tendency during 2016	GWL range	GWL tendency during 2016	Well depth/screened section	D18 isotopic signal (June 2016)
Z4-MS	Magarini s.	4	Shallow aquifer	04/2016–02/2017	311–380	Down	27.25–27.55	Down	29	−3.12
Z4-85	P. corals	4	Shallow aquifer	01/2016–04/2017	698–973	Stable	9.62–9.9	Down	10.4	−2.94
Z4-78	P. corals	4	Shallow aquifer	01/2016–04/2017	2418–2652	Stable	8.04–8.4	Not clear	No data	−2.74
Z4-24	Kilindini s.	3	Shallow aquifer	01/2016–03/2017	184–326	Not clear	6.21–7.65	Stable	7.5	−2.44
Z4-18	P. corals	4	Shallow aquifer	01/2016–04/2017	705–960	Stable	15.24–15.5	Stable	15.9	−3.14
Z4-11	Magarini s.	4	Shallow aquifer	01/2016–04/2017	102–621	Up	12.63–16.1	Down	17.87	−2.80
Z4-08	Kilindini s.	4	Shallow aquifer	01/2016–06/2016	585–768	Stable	23.38–27.69	Down	28	−3.17
Z4-06	Kilindini s.	4	Shallow aquifer	01/2016–12/2016	675–840	Stable	23.5–24.1	Down	24.6	−3.23
Z4-04	Kilindini s.	4	Shallow aquifer	01/2016–04/2017	538–644	Stable	22.62–23.5	Down	23.6	−3.00
Z4-01	Kilindini s.	4	Shallow aquifer	01/2016–04/2017	615–692	Stable	22.97–23.48	Down	No data	−3.24
Z3-98	P. corals	3	Shallow aquifer	01/2016–04/2017	728–920	Up	11.35–11.76	Stable	12	−2.59
Z3-96	P. corals	3	Shallow aquifer	01/2016–04/2016	2985–3090	Not clear	7.08–8.19	Not clear	8.3	−2.58
Z3-90	P. corals	3	Shallow aquifer	01/2016–04/2017	1674–3655	Up	6.22–8.49	Down	No data	−2.62
Z3-87	P. corals	3	Shallow aquifer	01/2016–04/2017	1659–2120	Up	4.84–5.1	Stable	No data	−2.59
Z3-30	Kilindini s.	2	Shallow aquifer	01/2016–04/2017	535–1375	Down	3.37–5.62	Down	No data	−2.54
Z3-29	Kilindini s.	2	Shallow aquifer	01/2016–04/2017	225–390	Down	9.94–11.13	Down	12.04	−2.68
Z3-102B	P. corals	2	Shallow aquifer	04/2016–04/2017	507–640	Up	11.24–11.8	Down	12	−2.40
Z2-112	Magarini s.	2	Shallow aquifer	01/2016–04/2017	55–128	Down	6.75–8.11	Down	No data	−2.40
Z2-104	P. corals	2	Shallow aquifer	01/2016–04/2017	628–697	Stable	No data	No data	No data	−2.64
Z2-103	P. corals	2	Shallow aquifer	01/2016–04/2017	606–900	Stable	11–11.51	Stable	No data	−2.69
Z1-70	Kilindini s.	1	Shallow aquifer	01/2016–04/2017	510–911	Down	2.73–5.44	Down	6.6	−2.29
Z1-33	Kilindini s.	1	Shallow aquifer	01/2016–04/2017	531–759	Up	9.86–10.47	Down	10.65	−2.64
Z1-140	Magarini s.	2	Shallow aquifer	01/2016–04/2017	529–669	Up	11.06–12.94	Stable	13.4	−3.12
Z1-135	Kilindini s.	2	Shallow aquifer	01/2016–04/2017	190–360	Down	3.18–5.05	Down	No data	−1.97
Z1-125	Magarini s.	1	Shallow aquifer	01/2016–04/2017	88–182	Up	14.11–16.99	Down	17.1	−2.70
Z1-124	Magarini s.	1	Shallow aquifer	01/2016–01/2017	207–350	Not clear	13.62–15.19	Not clear	15.2	−2.61
Z1-122	Magarini s.	1	Shallow aquifer	01/2016–04/2017	122–217	Down	10.82–12.82	Down	No data	−2.25
Z1-121	Kilindini s.	1	Shallow aquifer	01/2016–04/2017	560–671	Up	No data	No data	No data	−1.40
Z1-110	Kilindini s.	2	Shallow aquifer	01/2016–04/2017	92–206	Down	4.78–6.4	Down	6.4	−2.18
DB/FI/HP	Kambe	2	Deep aquifer	04/2016–04/2017	516–695	Stable	No data	No data	No data	−3.07
DB/BM/HP	Kambe	2	Deep aquifer	04/2016–04/2017	236–208	Stable	No data	No data	No data	−3.14
C/15/10	Mazeras snd.	1	Deep aquifer	04/2016–04/2017	379–677	Up	No data	No data	No data	−3.15
C/109/21	Mazeras snd.	2	Deep aquifer	04/2016–04/2017	483–790	Up	No data	No data	No data	−3.16
C/06/12	Mazeras snd.	1	Deep aquifer	04/2016–04/2017	248–760	Up	No data	No data	No data	−3.10

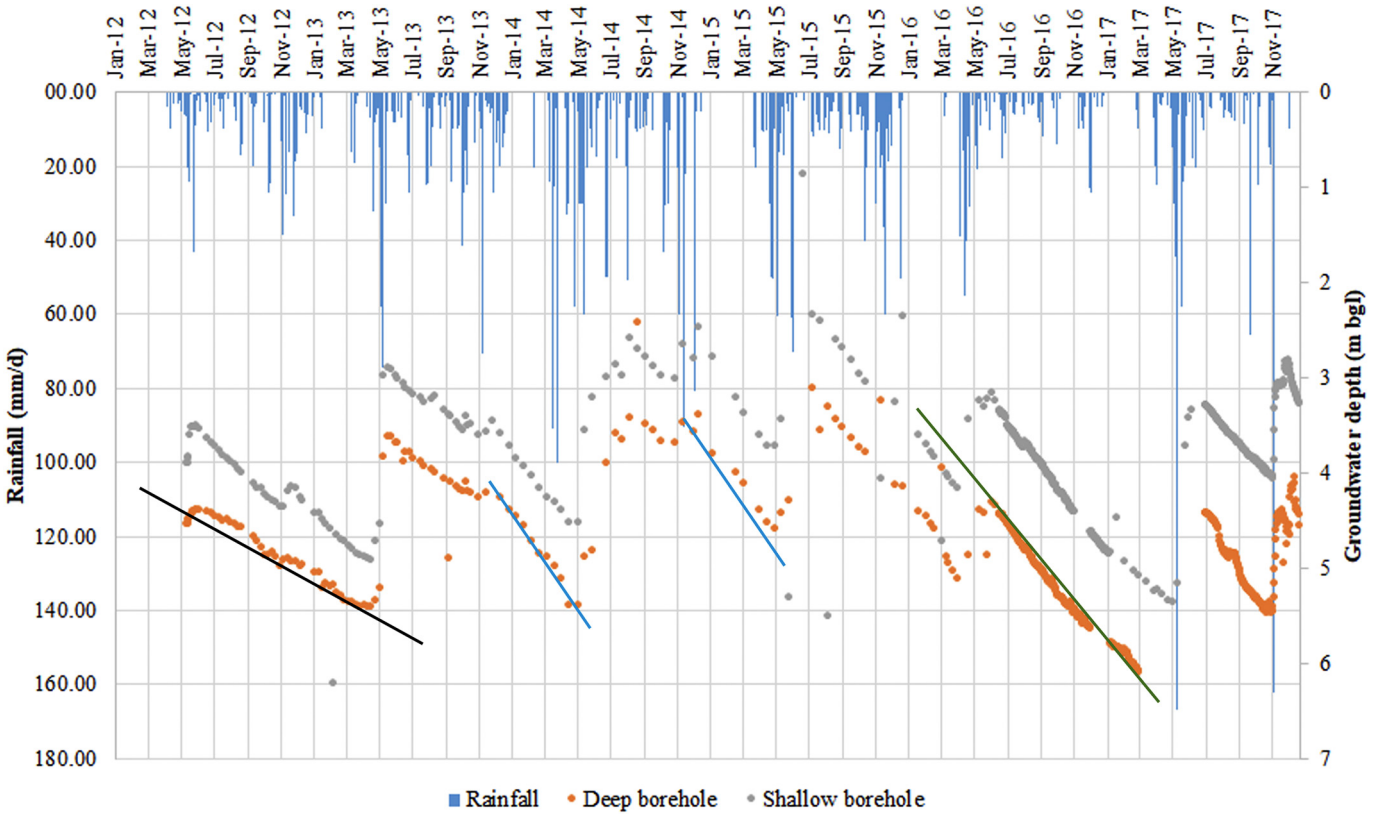

Fig. 7. Base Titanium shallow and deeper control piezometers at an elevation of 24.6 m asl. The black line shows the groundwater recession that occurred in 2012 and early 2013 under natural conditions, since the wellfield was not intensively pumped until October 2013. The blue lines show the reduction in groundwater level occurring between recharge events once abstraction had commenced. The green line shows the slope increment of groundwater recession possibly caused by increased abstraction during the La Niña event of 2016. The recession is taken as a line as the total drawdown is much smaller than the final stage controlled by the sea level. (For interpretation of the references to color in this figure legend, the reader is referred to the web version of this article.)

5.4. Hydrochemical facies

The survey having more points sampled (June 2016) was chosen to represent the hydrochemical results of the study area. Although two field campaigns were carried out and each one represents a different season (dry and wet), the year 2016 was very dry and recharge in the rainy season were lower than usual because of La Niña 2016/2017 event, as stated in Section 5.2 (Fig. 4).

Hydrochemical data shows the groundwater pattern in space and in depth. From it, the flow paths and the main hydrochemical processes that are taking place in the study area can be deduced. Based on hydrochemical datasets, some groundwater hydrochemical facies are defined according to their major ion content following the methodology presented in Anglés et al. (2017). A total of 5 hydrochemical groups are described according to geology and the hydrochemical facies (Figs. 8 and 9):

Hydrochemical group 'A' comprises samples with a Ca-HCO_3 facies that are hosted mainly in Pleistocene materials, Kilindini sands ('Pls') and Pleistocene corals ('Plc'), and a few samples from the deep aquifer in Mazeras sandstone (Fig. 8). This is the dominant group, comprising 63% of the samples. pH is over 6.0 (6.1 to and 7.2). Some samples of this group are saturated with respect to calcite, most of them located in the limestone materials closest to the shoreline (Table 3).

Other facies present in Pleistocene materials are Na-Cl waters, located on the coastal line around Gazi bay and north coast (Fig. 9). The group 'B' consists in 9% of the samples representing the points affected by the saline intrusion, which is also supported by the average EC around 2850 μS/cm and a maximum value of 4061 μS/cm. Furthermore, the ratio Na/Li of this samples follow the mixing sea water line (Line 1, Fig. 10b).

Group 'C' comprises 15% of the samples and has a Na-Ca-HCO_3 facies. Most samples in this group are located in the Mazeras sandstone outcropping at Shimba Hills and in their extension as the deep aquifer emplaced under the Magarini and Kilindini sands. These wells stand out by its lower Ca content, yet higher Na (Table 2) (Fig. 10a).

Group 'D' is represented by the 5% of the samples in Mazeras sandstone but having Na-Cl-HCO_3 facies. These samples are located up to Shimba Hills and they are enriched in Si (>20 mg/L Si or >40 mg/L SiO_2) (Table 2). The presence of quartz-feldspar minerals and silicified units in this formation with oversaturation relative to quartz (SI > 1) indicates that the main process governing the Si content in this water is silicate weathering (Table 3). The sample labeled Maji ya Chumvi beds (pink symbol) corresponds to a point located at Lukore, up to the Shimba Hills, which present also this kind of facies but with a greater concentration of HCO_3, Na and Cl than the other samples of the group. This Cl and Na enrichment can be due to the greater water retention depth in the soil, thus increasing evapo-concentration or due to the presence of bluish-black gritty shales and muddy sandstones with possible salt remnants deposited during a period of fluctuating climate. Hydrochemically, this sample does not follow the sodium enrichment line and moves out the left side (Fig. 10c), suggesting a process that incorporates further HCO_3 to groundwater from the soil gas (Armengol et al., 2017). A similar composition in sample C/12/12 points to connectivity between Triassic (Maji ya Chumvi Fm.) and Jurassic materials (Mazeras sandstone) (Fig. 10a).

Group 'E' represents the samples located in the Magarini sands (shallow aquifer) with Na-HCO_3-Cl facies. These samples also show high Si content and their Na concentration could come from silicate weathering process. However, these samples present the lowest ratio

Na/Li compared to the other facies (Fig. 10b) that could point a recharge area located in Magarini sands.

5.5. Water environmental isotopes

There is a relatively small change in altitude in the study area with a maximum elevation of 454 m asl at the Shimba Hills. Most of the samples follow the African Meteoric Water Line (AMWL) (Mckenzie et al., 2010). The samples present a deuterium excess between 8 and 13‰ relative to the Global Meteoric Water Line (GMWL) (Fig. 11a), which is the same deuterium excess obtained in Levin et al., 2009 for the coast of Kenya and Ethiopia. It may be indicative of precipitation formed from water vapor from an oceanic environment with less than average air humidity conditions, or alternatively from water evaporated near the land surface, either as a product of evaporated rainfall that recondenses or evaporation from surface water (Levin et al., 2009).

All samples from Shimba Hills (group 'D') and those of group 'E' in the Magarini sands have the lightest isotopic signal with $\delta^{18}O$ equal to $-3.15‰ \pm 0.21‰$ and $-3.07‰ \pm 0.25‰$ respectively. Most samples of the deep aquifer have the same isotopic composition as the samples from Shimba Hills (Fig. 11b).

The shallow aquifer has a heavier water isotopic composition due to its proximity to the coast and the lower altitude. Nevertheless, the shallow wells located in Kilindini formation in the north area present lighter isotopic values, similar to the samples from the deep aquifer. In addition, sample D/16/10 has a heavy isotopic value ($\delta^{18}O = -1.4‰$) and could be on a line of slope 4 (Fig. 11) corresponding to evaporation from a free water surface. This isotopic enrichment suggests the influence of water infiltrated from the seasonal Lake Nimbodze near the sampled point (Fig. 11b).

The isotopic composition of the samples from the rivers in the study area (Ramisi, Mukurumudzi and Mwachema Rivers) show evaporation effect, except the sample upstream of Mukurumudzi, located at the Shimba Hills (Fig. 11a).

5.6. Nitrogen pollution

One of the most common groundwater quality problems worldwide is nitrate pollution (Custodio, 2013). Typically, nitrate pollution in Africa comes from nitrogen compounds in wastewater and sewage (e.g. leakage from latrines into the aquifer), and from fertilizers applied in agriculture (Ouedraogo and Vanclooster, 2016); soil degradation and faecal contamination from extensive animal raising can also be factors. Most samples in the study area show low nitrate concentrations, under 5–10 mg/L NO_3 (Table 3), which may approach the chemical groundwater base-line. During March 2014 (dry season), only 2 out of 32 samples had nitrate concentration over the drinking water level limit of 50 mg/L. During the wet season in the same year, only one point had relatively high nitrate concentration, just below the drinking water limit. In 2016, when 75 (March) and 80 (June) groundwater points were sampled across the study area, samples with higher nitrate concentrations were also uncommon (Supplementary material). The small amount of points which show nitrate contamination are located in the main villages of Msambweni, Gazi and Ukunda, except point Z3-98 located east of the KISCOL sugar fields around Kinondo (Table 2). In village areas, the source of nitrate pollution in the samples

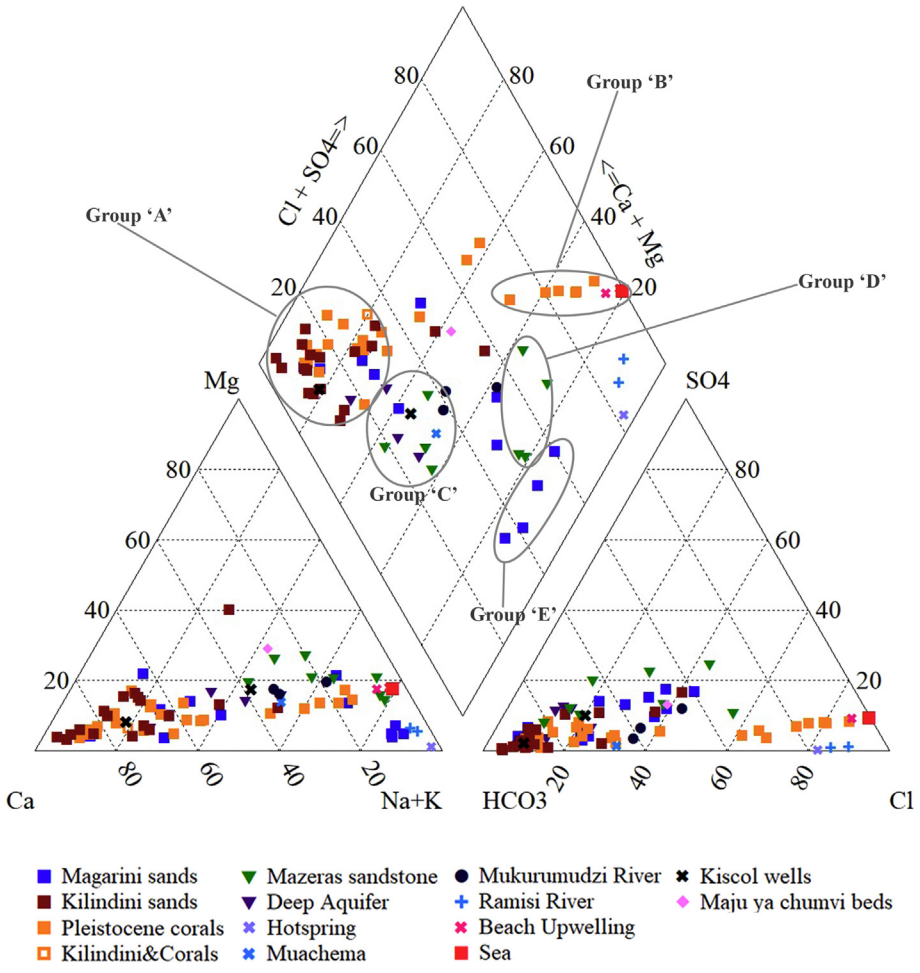

Fig. 8. Piper diagram of all points sampled during June 2016 field survey. The values are percentage of the cations over the total and anions over the total, for concentrations in meq/L.

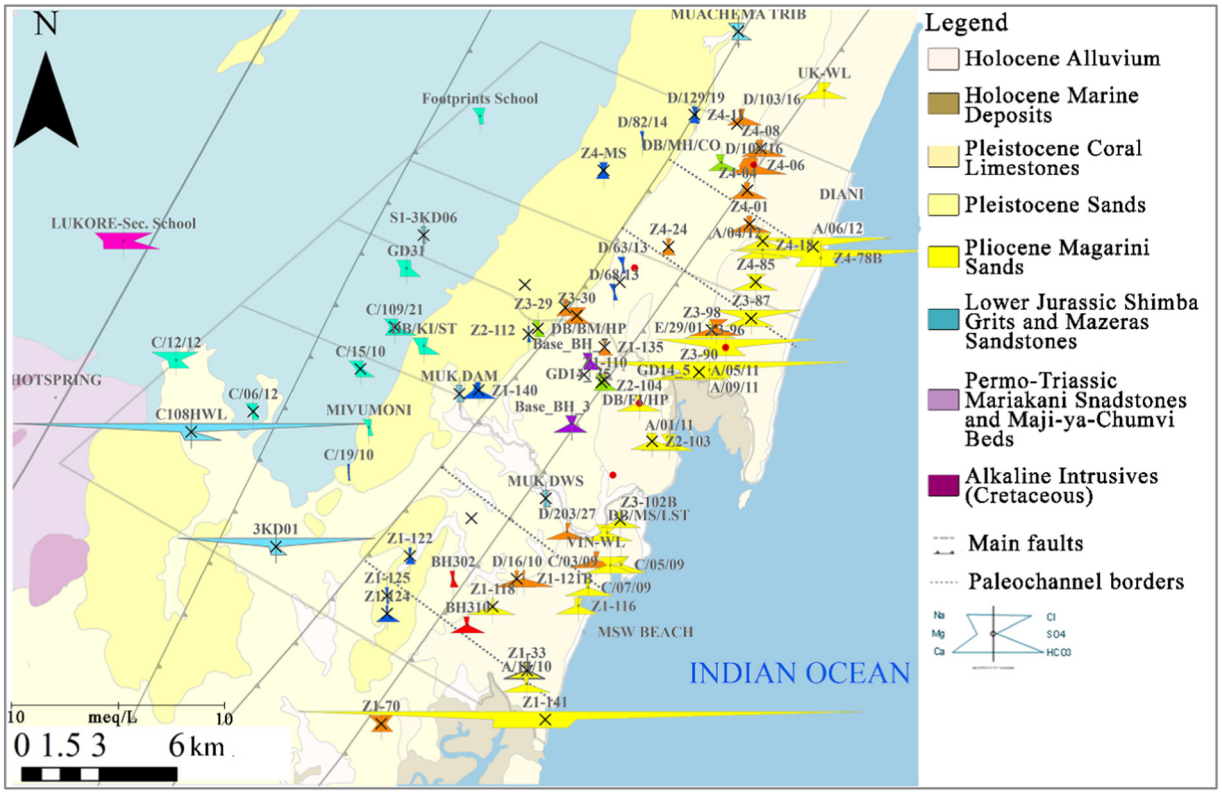

Fig. 9. Modified Stiff diagram for points sampled in June 2016. Crosses indicate points monitored fortnightly and red dots the points at which fortnightly sampling was cut down due to various problems. The purple and green modified Stiff diagrams correspond to samples from the deep confined aquifer. The yellow modified stiff diagrams correspond to samples located on Pleistocene corals, orange located in Kilindini sands and blue samples located in Magarini sands. The light green corresponds to the samples located in Mazeras Fm. and light blue samples from surface water. Red modified Stiff diagrams correspond to KISCOL samples. (For interpretation of the references to color in this figure legend, the reader is referred to the web version of this article.)

could be latrines or animal faeces. In the sugarcane plantation, nitrate pollution could be associated with fertilizer use. Overall, despite the potential for nitrate pollution due to poorly managed sewage/wastewater and growing agricultural activity in the study area, nitrate pollution seems so far to be locally confined. In 2014 and 2016 nitrate concentration was higher during the dry season than during the wet season, likely due to the lower rate of recharge in the dry season (see Folch et al., 2011; Menció et al., 2016). Recharge dilutes and transports local contamination down flow, while higher rates of nitrogen uptake as plants grow following precipitation also reduces nitrate concentration in the soil while it is in the root zone (Wick et al., 2012).

Some samples show significant concentrations of ammonia. During the dry season of 2016, 6 points had ammonia between 0.2 and >8 mg/L NH_4 and during the wet season, only 4 points presented ammonia of between 0.2 and 5 mg/L. Furthermore, there are points in several geological areas with values of Eh in the range of iron reduction (Table 2) (Faulwetter et al., 2009). The most reducing waters are those located in the middle area, in the Pleistocene corals and in the deep aquifer. Some of these points also have a high concentration of dissolved manganese and iron. Therefore, although there is no clear trend or distribution. Hydrochemical data seems to indicate potential reducing conditions across the study area, which could affect nitrate concentrations as ammonia is oxidized.

This assumption may be confirmed by the iron stability diagram (Supplementary material). All samples are located between the Fe^{+2} and $Fe_2O_3 \cdot nH_2O$ stability fields. The samples on the Fe^{+2} field are located on Mazeras sandstone and Magarini sands, i.e. in facies 'C', 'D' and 'E'. These facies present lower pH due to the absence of carbonates in the terrain and thus, boreholes in these areas produce more acid water, which has been seen to affect borehole/handpump functionality in these areas. The fact that significant dissolved oxygen (DO) concentrations were measured in many of these points (Table 2) indicates that there is no chemical equilibrium between dissolved oxygen, pH and Eh, but a kinetic situation due to recent mixing of waters.

Redox conditions could be influenced by the presence of organic matter. High concentration of dissolved organic carbon, measured as total organic carbon (TOC), was observed. Notably, the TOC value tends to increase toward the coast, with lower values inland. The samples with the highest TOC are located in Pleistocene corals (Table 2). It is possible that TOC is an input from the soil/surface since the high P_{CO2} values match those expected from degradation of soil organic matter. This could be affecting the redox conditions in the aquifer (Table 2). In order to understand potential natural attenuation processes, it is important to define first the baseline composition of the aquifer system as Manzano et al. (2007) did, and then apply other sources of information, such as nitrate isotope measurement or organic matter data.

5.7. Hydrochemical changes between seasons in 2014 (wet) and 2016 (La Niña) years

Comparing the 24 samples from March and June 2014 (wet year) field surveys, most fresh water samples (around 60%) were more saline during June than in March (Table 2a and b Supplementary material). However, the samples in the lower part of zone 4 do not present any variation between the two field campaigns. In contrast with 2014, in 2016 the fresh groundwater samples from the dry and wet seasons (March and June 2016 respectively) show similar salinities (Table 3 Supplementary material). However, there is an increase in salinity in the samples from groundwater affected by saline intrusion along the coastline, mainly on the north coast around Ukunda and Diani (Fig. 1).

Comparing hydrochemical data for the 22 points sampled in both wet seasons (June 2014 and June 2016 – the La Niña year of low

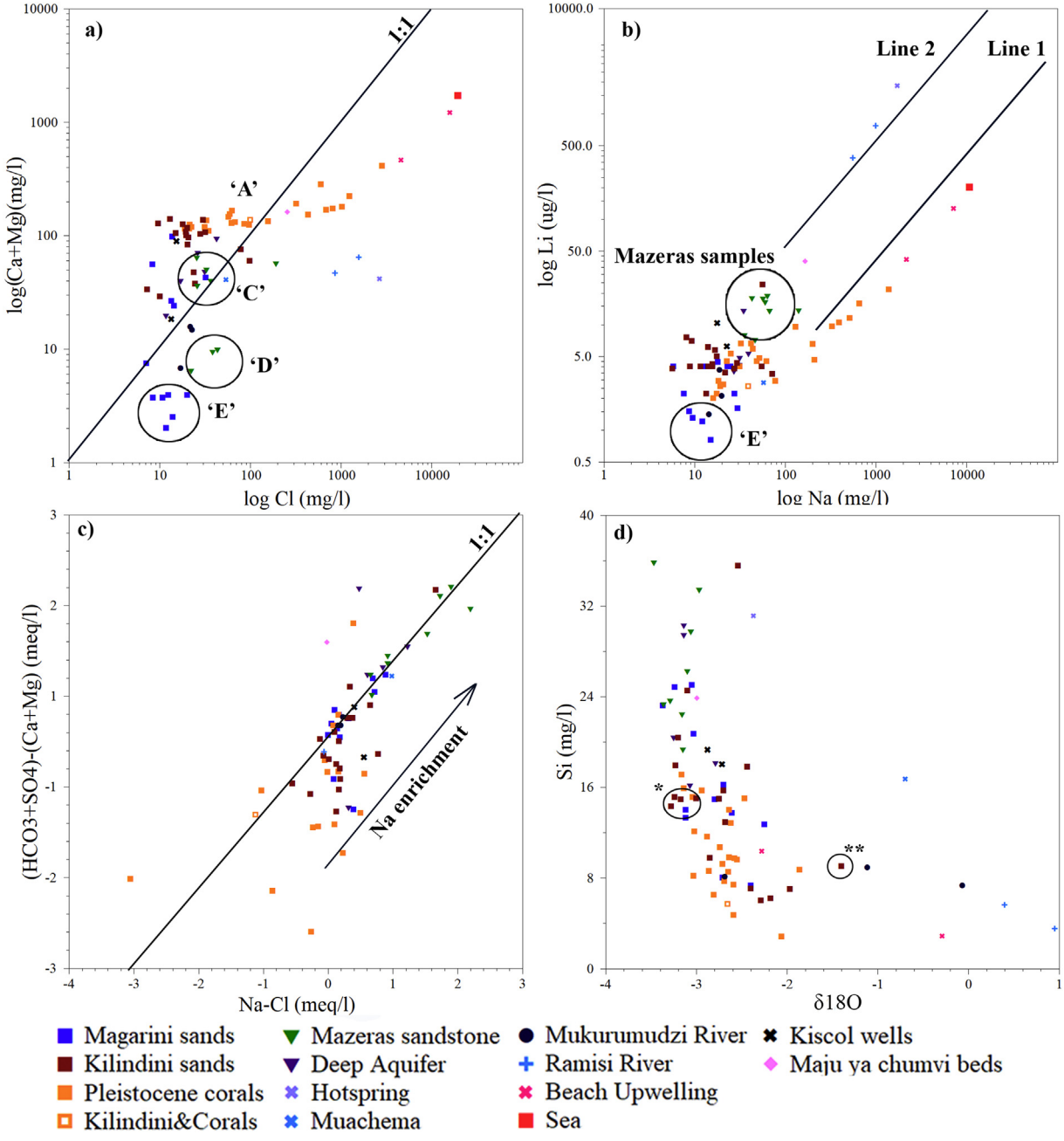

Fig. 10. a) Cl vs. log (Ca + Mg) in mg/L; b) log Li concentration (μg/L) vs. log Na in mg/L; c) (Na-Cl) vs. [(HCO_3 + SO_4)-(Ca + Mg)] in meq/L; d) Si vs. $\delta^{18}O$. *It is referred to the samples in zone 4 that present $\delta^{18}O < -3$. **It is referred to samples D/16/10.

rainfall), most of the fresh groundwater samples (around 60%) showed higher salinity during June 2014. The samples in zone 4 have the same hydrochemical composition in both years, with <2.4% average difference when comparing the concentration of the major ions between years and <6.3% average difference when comparing the EC values. However, the samples affected by saline intrusion (group 'B') present a 20% increment in salinization during La Niña year compared to that measured in June 2014.

6. Discussion

6.1. Conceptual flow model

The geophysical profiles allow a comprehensive three-dimensional understanding of the aquifer geometry of the study area and of vertical and lateral relationships through the geological formations. The groundwater level time series, hydrochemistry and water isotopes have helped to determine the main recharge areas, the connectivity between the geological formations and the consequences of drought on the groundwater system.

According to the stability diagrams of silicates (Supplementary material), weathering produces kaolinite as the main clay mineral in equilibrium with primary silicates for all the points sampled in the study area. This weathering product is preferentially formed under the climatic conditions dominating in the study area. Kaolinite is formed in rainy areas with intense rainfall and well-drained conditions (Appelo and Postma, 2005). Hydrochemical and isotopic data allow the definition of groundwater flow paths and main recharge areas, as in other studies under similar conditions (Anglés et al., 2017; Edmunds et al., 2003; Manzano et al., 2007; Menció et al., 2012). Different hydrochemical data facies illustrate the hydrochemical sequence that takes place within the system (Fig. 9).

Table 2
Physico-chemical parameters measured in the field and hydrochemical data for June 2016 field survey.

Code	Localization	Geology	Data	Cond. (μS/cm)	Tª (°C)	PH	TOC (mg/L)
FOOTPRINTS SCHOOL	Foot Print Children Home/School	Mazeras snd.	06/06/2016	311,7	27,5	5,8	0,9
Z4-11	Mabokoni Msikitini	Magarini s.	06/06/2016	205	29,0	6,6	0,9
Z4-01	Kiuzini	Kilindini s.	07/06/2016	671	29,2	7,0	0,9
A/04/12	Galu Chungoni	P. corals	07/06/2016	64,5	29,6	6,8	0,7
Z4-18	Mwabungo _ Chiungoni	P. corals	07/06/2016	881,0	29,3	7,0	1,1
A/06/12	Mvureni-Maweni	P. corals	07/06/2016	2743	29,5	7,1	1,0
Z4-78B	Neptune	P. corals	07/06/2016	3793	28,1	7,4	1,5
Z4-08	Ukunda Settlement Scheme	Kilindini s.	06/06/2016	406,1	29,6	6,8	1,8
Z4-06	Ukunda Settlement Scheme	Kilindini s.	06/06/2016	769	28,9	6,8	0,5
D/100/16	Ukunda Scheme Kwa Boga	Kilindini s.	06/06/2016	875	29,1	7,0	0,6
Z4-04	Mwabungo-Mwamua	Kilindini s.	07/06/2016	592	28,6	7,2	0,9
Z4-MS	Mkambani Mosque	Magarini s.	06/06/2016	364,1	28,4	6,5	0,7
D/82/14	Mwanjamba Kwa Mwakassim A	Magarini s.	06/06/2016	91,9	27,7	5,3	0,8
Z4-85	Kinondo	P. corals	07/06/2016	64,5	29,9	7,0	1,0
Z4-24	Kilole Primary School	Kilindini s.	08/06/2016	282,6	28,4	6,9	1,6
D/63/13	Zigira Chiyaye B	Magarini s.	08/06/2016	170,2	28,8	5,7	1,5
D/68/13	Zigira Bodo C	Magarini s.	08/06/2016	51,4	29,0	6,0	1,1
Z3-30	Magaoni Mosque	Kilindini s.	08/06/2016	735	29,2	6,8	
Z3-29	Mchenzani Magaoni	Kilindini s.	08/06/2016	342,2	28,1	6,7	1,4
DB/BM/HP	Bumamani	Kambe	08/06/2016	256,4	28,7	6,5	1.4
BH310	KISCOL Sugar Plantation	Mazeras snd.	23/06/2016	510	28,8	7,1	2,0
Z1-70	Darigube	Kilindini s.	13/06/2016	820	28,2	6,6	3,9
A/14/10	Munje Madukani	P. corals	13/06/2016	667	28,9	6,9	3,4
Z3-87	Kinondo	P. corals	07/06/2016	2011,0	29,2	6,9	1,0
Z3-98	Kinondo	P. corals	11/06/2016	830	28,8	6,9	2,9
Z3-90	Makongeni	P. corals	14/06/2016	2360	28,2	6,6	1,2
A/05/11	Makongeni Kambini	P. corals	14/06/2016	1750	30,3	6,8	1,7
HOTSPRING	Hotspring on the Tributary of Ramisi River	Spring	09/06/2016	15,792,0	58,8	7,9	1,7
C108HWL	Eshu Bridge - Ramisi river	SW	09/06/2016	5594,0	32,1	8,5	7,6
3KD01	Mwachande Bridge	SW	09/06/2016	3211	30,6	8,6	9,4
MUACHEMA TRIB	Mwachema River	SW	11/06/2016	505	25,0	7,3	14,9
S1-3KD06	Shimba Hills Pumping Station - Mukurumudzi river	SW	15/06/2016	140	22,6	6,4	3,0
GD31	Shimba Hills Secondary School BH	Mazeras snd.	15/06/2016	290	28,0	7,0	1,4
MUK DAM	Mukurumudzi River- Base T Dam	SW	15/06/2016	230	26,9	6,8	4,0
MUK DWS	Mukurumudzi River Kiscol Dam	SW	15/06/2016	210	26,3	6,8	5,5
Z1-122	Kidzumbani	Magarini s.	10/06/2016	210	27,9	6,3	1,5
Z1-125	Gongonda	Magarini s.	10/06/2016	112	27,6	5,3	1,2
Z1-124	Gongonda	Magarini s.	10/06/2016	325,3	28,9	6,5	1,7
D/16/10	Milalani-Nimbodze kwa Mwabiti	Kilindini s.	10/06/2016	592	28,7	6,6	1,5
Z1-121B	Milalani	Kilindini s.	10/06/2016	589	28,4	6,5	1,6
Z1-116	Mwaembe	P. corals	15/06/2016	740	30,0	6,8	2,0
C/07/09	Kisimachande	P. corals	10/06/2016	666	30,1	6,6	1,9
A/01/11	Gazi Mezea	P. corals	14/06/2016	1040,0	29,1	6,7	1,4
Z2-103	Gazi shallow well	P. corals	11/06/2016	890	28,8	7,0	3,8
D/203/27	Marigiza - Baa Kanda (Voroni)	Kilindini s.	14/06/2016	610	30,7	6,7	1,4
DB/MS/LST	Vingujini opp Msambweni Police	P. corals	13/06/2016	1010	29,8	6,8	4,1
Z1-135	Madzi Kuko Centre	Kilindini s.	08/06/2016	253,9	27,6	7,2	1.4
Z2-112	Bumamani	Magarini s.	08/06/2016	41,3	27,6	6,1	1,4
Z1-140	Vumbu	Magarini s.	15/06/2016	650,0	28,3	6,7	1,8
Z2-104	Sala center	P. corals	16/06/2016	610	29,2	6,7	2,1
Z1-110	Fihoni Primary School	Kilindini s.	16/06/2016	180	30,5	7,2	2,6
DB/FI/HP	Fihoni Chief's camp	Kambe	16/06/2016	590,0	30,6	7,2	2,0
Z3-96	Kinondo	P. corals	11/06/2016	3300	28,9	7,0	173,3
E/29/01	Kinindo Amani Mosque	Pls-Plc	11/06/2016	980	29,2	6,7	3,2
A/09/11	Makongeni Bandani	P. corals	14/06/2016	475	30,1	7,0	1,2
MIVUMONI	Mivumoni Secondary School (BH)	Mazeras snd.	15/06/2016	260	29,1	5,7	1,9
C/15/10	Mivumoni	Mazeras snd.	09/06/2016	66,4	27,8	6,4	1,5
C/109/21	Amka village	Mazeras snd.	15/06/2016	630	27,2	6,6	1,4
C/12/12	Maphombe Primary	Mazeras snd.	09/06/2016	65,7	29,1	6,4	
C/06/12	Gazore	Mazeras snd.	09/06/2016	313	27,8	5,7	1,6
C/19/10	Mivumoni-Makutano	Magarini s.	09/06/2016	42,7	28,0	5,3	1,6
D/129/19	Mabokoni Msikitini	Magarini s.	06/06/2016	49,2	27,9	5,9	0,4
DB/MH/CO	Muhaka I.C.P.E. Coastal Field St	Mazeras snd.	07/06/2016	516	29,3	7,2	0,4
Z1-141	Jabalini	P. corals	13/06/2016	9440	28,0	6,9	4,4
UK-WL	Ukunda hand dug well	P. corals	11/06/2016	1040	29,2	6,7	2,6
D/103/16	Ukunda Scheme Kwa Madzugwe	Kilindini s.	06/06/2016	539,0	28,7	7,0	0,7
LUKORE-SEC. SCHOOL	LUKORE-SH	Mazeras snd.	09/06/2016	70,0	27,7	6,7	1,5
Z1-118	Mabatani	P. corals	10/06/2016	710,0	28,7	6,5	1,6
VIN-WL	Vingujini well	Kilindini s.	13/06/2016	780,0	29,6	6,7	4,4
BASE_BH_3	Base Titanium	Mazeras snd.	17/06/2016	590,0	28,1	6,9	3,0
BASE_BH_7	Base Titanium	Mazeras snd.	17/06/2016	370,0	28,6	6,7	3,3
DB/KI/ST	Kibwaga Feeder School	Mazeras snd.	18/06/2016	500	27,5	6,58	2375
Z3-102B	Nyumba Sita	P. corals	16/06/2016	540,0	29,6	7,0	2,8
BH302	KISCOL Sugar Plantation	Mazeras snd.	23/06/2016	200,0	29,6	6,5	1,8
DIANI	Diani Beach	SW	22/06/2016	46,750,0	27,3	7,0	3,7
MSW BEACH	Masabweni Beach	SW	22/06/2016	12,250,0	29,1	6,9	3,7
C/05/09	Vingujini	P. corals	24/06/2016	894,0	28,3	6,9	1,9
C/03/09	Vingujini	P. corals	24/06/2016	1435,0	28,5	6,9	2,1

Alkalinity (as mg/L HCO_3)	HCO_3	DO (mg/L)	ORP (mV)	EH (mV)	NH_4 (mg/L)	Cl (mg/L)	SO_4 (mg/L)
						0.042 mg/L	0.026 mg/L
54,9	54,9	2,2	−26,5	193,5	0,0	43,3	33,2
79,3	79,3	7,9	38,4	258,4	0,0	13,5	4,5
317,3	317,3	5,4	71,2	291,2	0,0	20,0	13,0
396,6	396,6	5,8	93,5	313,5	0,0	62,3	27,5
366,1	366,1	6,5	33,0	253,0	0,0	68,3	24,9
311,2	311,2	7,1	−39,6	180,4	0,0	690,1	86,1
256,3	256,3	6,1	34,9	254,9	0,0	1025,2	132,6
378,3	378,3	4,5	7,9	227,9	0,0	19,4	3,8
396,6	396,6	3,7	61,5	281,5	0,0	17,9	3,3
488,2	488,2	3,1	50,4	270,4	0,0	28,0	26,6
292,9	292,9	5,7	25,5	245,5	0,0	20,9	15,6
85,4	85,4	5,8	44,8	264,8	0,0	32,2	19,5
18,3	18,3	7,9	136,2	356,2	0,0	11,7	6,0
317,3	317,3	6,1	65,8	285,8	0,0	85,6	16,1
103,7	103,7	3,5	−58,0	162,0	0,0	24,6	2,2
42,7	42,7	2,9	88,3	308,3	0,0	20,0	8,2
54,9	54,9	3,0	−5,8	214,2	0,0	10,8	9,3
189,2	189,2	3,9	52,5	272,5	0,0	78,3	30,8
115,9	115,9	4,3	45,6	265,6	0,0	23,9	14,8
109,8	109,8	5,3	91,0	311,0	0,0	11,8	14,6
262,4	262,4	3,8	56,8	276,8	0,0	15,4	4,8
177,0	177,0	5,4	−120,8	99,2	0,0	98,7	54,0
353,9	353,9	3,9	80,0	300,0	0,0	21,6	6,0
335,6	335,6	5,5	47,1	267,1	0,0	433,2	49,7
347,8	347,8	7,2	40,7	260,7	0,0	33,0	2,1
433,2	433,2	5,5	−33,3	186,7	0,0	602,5	41,8
305,1	305,1	3,3	−32,0	188,0	0,0	320,8	29,0
976,3	976,3	0,9	−197,0	23,0	5,0	2642,7	<LOQ
445,4	445,4	11,6	−18,3	201,7	1,2	1561,9	16,7
158,7	158,7	8,9	−32,5	187,5	0,0	858,9	11,9
189,2	189,2	5,1	−30,6	189,4	0,0	53,5	2,6
30,5	30,5	8,6	66,8	286,8	0,0	16,9	6,3
207,5	207,5	4,3	−77,9	142,1	0,0	32,8	51,7
61,0	61,0	7,4	−36,3	183,7	0,0	21,6	5,2
67,1	67,1	8,2	32,3	252,3	0,0	22,4	2,8
79,3	79,3	7,6	51,2	271,2	0,0	14,4	2,3
30,5	30,5	5,4	111,9	331,9	0,0	12,5	4,3
189,2	189,2	2,2	23,3	243,3	0,5	8,3	6,5
286,8	286,8	3,4	52,8	272,8	0,0	15,0	6,5
433,2	433,2	5,2	25,5	245,5	0,0	13,0	0,3
292,9	292,9	3,2	58,7	278,7	0,0	31,4	14,6
378,3	378,3	3,4	−9,1	210,9	0,0	22,4	10,8
360,0	360,0	1,1	31,2	251,2	1,2	57,3	31,3
396,6	396,6	5,6	−69,4	150,6	0,0	34,9	31,8
292,9	292,9	3,3	−3,3	216,7	0,0	31,9	2,1
372,2	372,2	1,4	−180,9	39,1	0,8	97,4	15,9
122,0	122,0	7,1	−25,8	194,2	0,0	7,3	3,1
36,6	36,6	5,6	93,8	313,8	0,0	7,1	1,6
256,3	256,3	1,0	−92,0	128,0	0,0	13,8	15,0
317,3	317,3	2,1	−42,6	177,4	0,0	19,0	13,8
85,4	85,4	3,0	−56,8	163,2	0,0	10,1	9,2
244,1	244,1	0,8	−96,7	123,3	0,0	31,4	32,0
292,9	292,9	3,6	−221,0	−1,0	0,0	810,8	110,6
360,0	360,0	3,7	−9,4	210,6	0,0	99,9	8,6
323,4	323,4	1,8	−21,1	198,9	0,0	1241,2	166,7
61,0	61,0	1,8	64,2	284,2	0,0	22,2	22,6
207,5	207,5	1,7	−134,3	85,7	0,2	25,9	27,0
317,3	317,3	1,1	−178,7	41,3	0,0	25,6	24,5
195,3	195,3	1,6	0,7	220,7	0,0	192,4	50,0
85,4	85,4	2,5	87,7	307,7	0,0	38,5	18,1
18,3	18,3	2,6	52,6	272,6	0,0	8,4	5,4
48,8	48,8	4,1	87,5	307,5	0,0	13,9	8,5
268,5	268,5	5,2	48,7	268,7	0,0	26,2	9,2
329,5	329,5	3,8	32,2	252,2	0,0	2852,4	359,6
335,6	335,6	6,6	70,3	290,3	0,0	59,7	14,4
286,8	286,8	4,3	90,6	310,6	0,0	20,3	2,3
543,1	543,1	1,6	90,5	310,5	0,0	253,8	114,8
335,6	335,6	3,4	−21,5	198,5	0,0	9,6	1,1
378,3	378,3	5,7	45,9	265,9	0,0	30,2	5,6
219,7	219,7	0,8	−126,3	93,7	0,0	42,5	15,9
183,1	183,1	4,1	−28,8	191,2	0,0	17,0	21,4
238,0	238,0	3,3	−127,0	93,0	0,0	36,8	26,8
299,0	299,0	7,0	5,8	225,8	0,0	19,7	2,1
79,3	79,3	2,7	40,3	260,3	0,0	13,4	8,9
177,0	177,0	4,4	101,6	321,6	0,0	15,844,0	2208,2
439,3	439,3	4,7	58,0	278,0	0,0	4570,0	651,6
384,4	384,4	2,7	40,3	260,3	0,0	62,7	9,2
353,9	353,9	4,2	154,2	374,2	0,0	157,1	27,5

(*continued on next page*)

Table 2 (*continued*)

Code	NO_3 (mg/L)	PO_4 (mg/L)	Br (mg/L)	F (mg/L)	Ca (mg/L)	Mg (mg/L)	Na (mg/L)
	0.005 mg/L	0,008 mg/L	0.004 mg/L	0.024 mg/L	0.05 mg/L	0.05 mg/L	0.1 mg/L
FOOTPRINTS SCHOOL	0,3	0,1	0,3	0,1	3,0	6,8	43,2
Z4-11	1,0	0,0	0,1	0,0	25,6	0,8	12,9
Z4-01	2,0	0,0	0,1	0,2	107,1	9,3	16,8
A/04/12	2,1	0,0	0,5	0,2	114,4	13,9	42,2
Z4-18	3,6	0,0	0,4	0,2	117,0	13,2	43,9
A/06/12	6,1	0,0	5,7	0,2	133,5	34,0	327,4
Z4-78B	11,8	0,0	4,1	0,2	125,0	54,1	510,8
Z4-08	1,8	0,1	0,2	0,1	94,7	12,9	27,5
Z4-06	0,5	0,0	0,2	0,2	108,6	15,9	29,3
D/100/16	0,1	0,0	0,5	0,7	58,6	44,0	56,4
Z4-04	1,2	0,0	0,2	0,1	84,5	11,0	17,5
Z4-MS	6,9	0,0	0,2	0,0	36,8	5,7	23,0
D/82/14	0,9	0,0	0,1	0,0	1,3	0,7	15,1
Z4-85	3,1	0,0	1,2	0,1	115,0	11,1	51,9
Z4-24	0,8	0,0	0,1	0,1	35,7	1,8	14,3
D/63/13	4,5	0,0	0,1	0,0	3,2	0,7	29,6
D/68/13	2,6	0,0	0,1	0,0	2,9	0,8	27,4
Z3-30	37,3	0,1	0,3	0,1	64,7	10,5	54,9
Z3-29	2,1	0,0	0,1	0,0	44,7	2,7	15,7
DB/BM/HP	0,3	0,3	0,1	0,1	15,0	4,5	27,3
BH310	9,4	0,1	0,1	0,2	83,2	5,5	22,6
Z1-70	41,4	0,0	0,2	0,0	49,0	10,4	71,8
A/14/10	6,1	0,0	0,1	0,1	120,3	3,8	17,6
Z3-87	17,2	0,0	2,1	0,1	130,2	22,5	210,7
Z3-98	73,1	<LOQ	3,8	0,1	132,4	3,2	16,1
Z3-90	1,6	0,0	2,1	0,1	257,7	24,5	200,9
A/05/11	5,5	0,0	1,0	0,1	174,6	16,1	130,0
HOTSPRING	0,2	0,1	8,5	8,9	32,9	8,2	1715,3
C108HWL	0,3	<LOQ	5,7	4,1	32,1	31,6	997,5
3KD01	0,2	0,0	4,6	2,1	25,3	21,0	555,3
MUACHEMA TRIB	0,3	0,0	0,2	0,1	32,3	8,2	57,2
S1-3KD06	1,5	0,0	0,1	0,0	4,1	2,6	14,3
GD31	1,2	0,1	0,2	0,2	31,7	17,9	56,5
MUK DAM	0,9	0,0	0,1	0,1	11,8	3,8	18,5
MUK DWS	0,5	0,0	0,1	0,1	11,2	3,4	19,6
Z1-122	20,8	0,0	0,1	0,0	21,5	2,4	9,5
Z1-125	6,6	0,0	0,1	0,0	2,6	1,3	12,1
Z1-124	9,9	0,0	0,1	0,0	54,1	1,5	7,6
D/16/10	4,5	0,0	0,0	0,1	100,9	3,5	14,1
Z1-121B	1,4	0,0	0,1	0,1	136,0	3,4	5,7
Z1-116	3,5	0,0	0,1	0,2	109,0	9,2	22,7
C/07/09	4,5	0,0	0,2	0,2	112,3	5,7	18,3
A/01/11	64,7	0,0	0,2	0,1	138,8	6,8	48,7
Z2-103	6,1	0,0	0,2	0,1	104,5	4,7	31,6
D/203/27	18,2	0,0	0,1	0,1	102,9	3,1	8,1
DB/MS/LST	0,3	0,0	0,3	0,2	107,9	15,6	62,0
Z1-135	3,1	0,0	0,1	0,1	30,4	2,9	11,6
Z2-112	0,8	<LOQ	0,0	0,0	6,6	0,8	5,8
Z1-140	0,2	0,0	0,1	0,2	80,3	17,0	18,0
Z2-104	2,1	0,0	0,1	0,1	107,7	6,5	25,2
Z1-110	3,7	<LOQ	0,1	0,1	27,9	0,9	8,9
DB/FI/HP	0,2	0,1	0,1	0,2	39,3	8,2	31,4
Z3-96	5,7	0,0	3,4	0,1	127,6	44,6	391,6
E/29/01	1,7	<LOQ	0,5	0,1	130,2	6,6	39,0
A/09/11	0,0	0,0	4,7	0,2	131,6	89,3	655,5
MIVUMONI	9,2	0,1	0,1	0,1	2,8	3,6	35,5
C/15/10	0,4	0,3	0,6	0,2	22,6	13,2	67,4
C/109/21	0,3	0,0	0,1	0,1	48,5	15,1	60,2
C/12/12	4,9	0,2	0,8	0,2	31,9	24,7	140,3
C/06/12	8,3	0,2	0,3	0,1	4,1	5,3	46,2
C/19/10	4,1	0,0	0,1	0,0	2,0	1,7	8,7
D/129/19	1,0	0,0	0,1	0,1	1,8	0,7	25,0
DB/MH/CO	3,4	0,1	0,1	0,1	63,5	6,5	31,0
Z1-141	1,5	<LOQ	10,3	0,1	257,5	151,9	1393,2
UK-WL	55,0	0,0	0,9	0,2	133,4	20,0	32,7
D/103/16	1,1	0,1	0,2	0,1	73,32	9,37	21,77
LUKORE-SEC. SCHOOL	3,4	0,1	1,3	0,1	98,96	61,21	164,12
Z1-118	3,7	0,0	0,0	0,1	124,75	2,59	9,28
VIN-WL	14,4	0,0	0,1	0,1	131,41	5,43	13,40
BASE_BH_3	0,4	0,1	0,2	0,1	88,12	4,98	34,91
BASE_BH_7	1,8	0,1	0,1	0,2	32,80	6,79	39,20
DB/KI/ST	0,8	0,0	0,3	<LOQ	21,60	17,73	63,71
Z3-102B	10,7	0,0	0,1	0,1	93,23	7,14	15,72
BH302	6,3	0,0	0,1	0,1	14,33	3,92	17,79
DIANI	0,8	0,0	58,7	0,7	334,91	878,22	7138,30
MSW BEACH	1,1	0,0	16,5	0,3	186,98	271,84	2167,80
C/05/09	51,8	0,03	0,2	0,1	158,58	6,58	20,90
C/03/09	16,4	0,03	0,5	0,1	122,60	10,90	78,08

K (mg/L)	Fe (mg/L)	Si (mg/L)	Al (mg/L)	Li (ppb)	Mn (ppb)
0.1 mg/L	0.05 mg/L	0.02 mg/L	0.05 mg/L	0.08 ppb	0.08 ppb
4,4	2,27	35,8	0,00	17,8	144,5
0,6	0,00	14,9	−0,04	<0,8	11,5
2,6	0,04	15,1	−0,08	5,7	4,4
4,2	0,05	17,1	−0,08	6,6	0,8
3,5	0,03	15,9	−0,03	5,9	2,1
8,6	0,18	10,7	−0,06	9,6	5,8
16,6	0,03	8,5	−0,04	11,5	12,5
2,5	0,01	14,9	−0,09	3,8	14,2
2,7	0,04	17,9	−0,03	4,3	12,6
2,4	0,00	14,3	−0,02	23,8	3,3
3,5	0,04	15,0	−0,09	5,0	8,5
1,8	0,03	13,3	−0,14	<0,8	16,6
2,0	0,03	25,0	−0,06	0,8	10,3
2,5	0,00	15,7	−0,06	4,8	2,6
1,3	0,02	17,8	−0,05	<0,8	102,5
1,6	0,03	23,2	−0,06	1,6	12,8
1,6	0,45	24,8	−0,13	2,2	8,8
8,4	−0,02	35,5	−0,09	<0,8	90,2
2,6	0,13	12,9	−0,02	4,2	7,3
2,3	0,05	29,4	−0,08	3,6	2,3
2,2	0,03	18,0	0,03	6,2	2,0
28,2	0,03	6,0	−0,04	3,4	43,7
1,4	0,02	8,6	0,02	2,2	1,1
5,9	0,03	7,4	−0,09	4,6	0,8
0,4	0,00	4,7	−0,02	2,0	2,6
5,9	0,18	12,8	0,20	6,5	14,1
5,6	0,07	15,0	0,17	9,5	21,8
61,0	0,07	31,1	−0,02	1832,0	48,3
30,1	−0,01	3,5	−0,07	764,8	55,3
15,4	0,18	5,6	0,03	379,0	212,4
5,9	0,08	16,7	−0,09	2,8	312,0
2,2	0,02	8,1	−0,12	1,4	68,6
5,7	0,85	23,3	−0,06	17,5	836,5
3,5	0,06	7,3	−0,01	3,7	155,8
2,0	0,23	8,9	0,00	2,1	231,7
0,5	0,03	12,7	−0,11	1,3	9,1
1,3	0,03	16,2	−0,10	1,2	34,3
1,8	0,01	13,7	−0,05	2,2	16,5
4,7	−0,04	9,0	−0,08	6,1	0,9
0,5	0,00	24,5	−0,03	3,8	1,8
2,5	0,04	12,1	0,04	4,5	4,5
1,5	0,01	9,6	−0,04	2,9	0,9
10,1	0,02	9,2	0,06	4,5	1,7
48,6	0,06	7,7	−0,01	4,0	9,2
1,3	0,06	15,7	0,07	7,5	4,0
6,1	2,12	11,6	−0,04	4,5	467,4
7,2	0,05	7,0	−0,13	<0,8	16,6
0,8	0,00	7,3	−0,10	<0,8	7,0
9,1	0,16	14,0	0,08	4,4	110,6
2,0	0,08	14,0	0,08	5,3	3,7
1,1	0,04	6,2	0,02	<0,8	9,1
2,0	0,03	16,1	−0,06	4,8	41,8
11,7	0,03	9,7	−0,06	10,4	11,6
1,6	0,00	5,7	−0,07	2,6	2,4
28,6	0,05	8,7	0,02	15,8	2,6
2,8	0,07	29,7	−0,06	7,9	93,0
3,9	0,78	19,3	−0,09	13,4	186,7
4,7	5,70	22,4	0,01	16,3	73,6
4,6	0,07	33,4	−0,12	13,6	267,5
5,0	0,02	26,2	−0,12	7,1	6,8
1,5	2,82	8,0	−0,10	1,5	52,7
0,8	0,12	20,7	−0,03	<0,8	5,9
2,7	−0,01	18,1	−0,10	4,1	<0,8
40,0	0,01	2,8	0,13	21,4	12,8
3,5	0,03	15,1	−0,01	6,6	3,4
3,45	0,05	20,34	−0,05	3,5	1,6
10,33	0,20	23,86	−0,07	39,7	68,2
1,07	0,04	14,94	−0,02	7,0	5,9
1,46	0,01	9,77	0,02	2,2	6,7
3,87	0,13	20,34	−0,06	13,4	112,1
3,03	0,08	30,24	−0,01	5,3	12,3
3,27	0,84	23,61	−0,01	18,6	225,4
3,65	0,02	7,04	−0,01	<0,8	<0,8
2,17	0,11	19,27	0,09	10,3	4,9
268,35	0,08	2,84	0,23	126,1	16,0
81,47	0,01	10,34	0,07	41,3	3,4
1,64	0,05	8,18	0,15	2,7	5,4
2,89	0,07	6,49	0,19	2,9	1,6

Table 3
Isotopic data from March and June 2016 field survey; saturation index of calcite and quartz for June 2016 field samples and ionic relation for June 2016 field survey.

Code	Data	$\delta^{18}O$	$\delta^{2}H$	Data	$\delta^{18}O$	$\delta^{2}H$	SI calcite	SI quartz	Na/Cl	Ca/HCO_3
FOOTPRINTS SCHOOL	06/06/2016	−3.47	−13.35	01/03/2016	−3.43	−13.51	−3.34	0.72	1.54	0.16
Z4-11	06/06/2016	−2.80	−9.79	01/03/2016	−2.87	−10.13	−1.40	0.32	1.46	0.98
Z4-09	–	–	–	02/03/2016	−3.14	−12.88	–	–	–	–
Z4-01	07/06/2016	−3.24	−13.56	02/03/2016	−3.50	−13.72	0.10	0.32	1.30	1.03
A/04/12	07/06/2016	−3.16	−13.30	06/03/2016	−3.30	−13.77	0.00	0.37	1.04	0.88
Z4-18	07/06/2016	−3.14	−12.87	06/03/2016	−2.98	−12.70	0.18	0.34	0.99	0.97
A/06/12	07/06/2016	−2.74	−10.92	06/03/2016	−2.66	−11.30	0.16	0.17	0.73	1.31
Z4-78B	07/06/2016	−2.65	−9.94	06/03/2016	−2.39	−10.01	0.28	0.09	0.77	1.49
Z4-08	06/06/2016	−3.17	−14.02	02/03/2016	−3.47	−13.89	−0.07	0.31	2.19	0.76
Z4-06	06/06/2016	−3.23	−13.84	02/03/2016	−3.42	−13.50	−0.01	0.40	2.53	0.84
D/100/16	06/06/2016	−3.28	−13.58	02/03/2016	−3.52	−13.59	−0.01	0.30	3.10	0.37
Z4-04	07/06/2016	−3.00	−12.67	02/03/2016	−3.15	−13.41	0.17	0.33	1.30	0.88
Z4-MS	06/06/2016	−3.12	−13.03	01/03/2016	−3.34	−13.56	−1.37	0.28	1.10	1.31
D/82/14	06/06/2016	−3.05	−12.46	01/03/2016	−3.31	−13.24	−4.60	0.56	1.98	0.22
Z4-85	07/06/2016	−2.94	−12.46	06/03/2016	−2.83	−11.82	0.12	0.33	0.94	1.11
Z4-24	08/06/2016	−2.44	−8.31	05/03/2016	−2.49	−8.07	−0.87	0.40	0.90	1.05
Z3-25	–	–	–	05/03/2016	−2.31	−7.85	–	–	–	–
D/63/13	08/06/2016	−3.37	−14.04	05/03/2016	−3.42	−14.73	−3.46	0.51	2.28	0.23
D/68/13	08/06/2016	−3.24	−14.06	05/03/2016	−3.37	−14.49	−3.09	0.54	3.90	0.16
Z3-30	08/06/2016	−2.54	−8.11	03/03/2016	−2.54	−7.75	−0.54	0.69	1.08	1.04
Z3-29	08/06/2016	−2.68	−9.52	03/03/2016	−2.83	−9.32	−0.95	0.27	1.01	1.18
DB/BM/HP	08/06/2016	−3.14	−12.22	03/03/2016	−3.25	−11.09	−1.62	0.62	3.57	0.42
BH310	23/06/2016	−2.72	−9.80	04/03/2016	−2.94	−11.64	0.03	0.40	2.27	0.97
BH402	–	–	–	04/03/2016	−2.78	−10.67	–	–	–	–
NK-03	–	–	–	04/03/2016	−2.86	−10.84	–	–	–	–
Z1-70	13/06/2016	−2.29	−7.52	11/03/2016	−2.42	−7.14	−0.91	−0.07	1.12	0.84
Z1-33	13/06/2016	−2.64	−9.28	11/03/2016	−2.72	−10.02	0.21	0.16	1.38	1.32
A/14/10	13/06/2016	−2.86	−10.59	11/03/2016	−2.90	−10.69	0.09	0.08	1.26	1.04
Z3-87	07/06/2016	−2.59	−9.17	06/03/2016	−2.78	−9.29	0.01	0.01	0.75	1.18
Z3-98	11/06/2016	−2.59	−8.46	08/03/2016	−2.72	−9.69	0.10	−0.18	0.75	1.16
Z3-90	14/06/2016	−2.62	−9.24	08/03/2016	−2.78	−10.37	0.06	0.27	0.51	1.81
A/05/11	14/06/2016	−2.47	−9.48	01/03/2016	−3.16	−11.69	0.03	0.30	0.63	1.75
HOTSPRING	09/06/2016	−2.37	−9.64	10/03/2016	−2.24	−8.94	0.97	0.24	1.00	0.10
C108HWL	09/06/2016	0.95	6.13	10/03/2016	1.85	7.66	0.98	−0.38	0.99	0.22
3KD01	09/06/2016	0.40	4.04	10/03/2016	2.78	11.48	0.62	−0.16	1.00	0.49
TIWI 8.2	18/06/2016	−2.94	−13.04	15/03/2016	−3.12	−13.98	−0.74	0.50	0.94	0.86
TIWI 1	14/06/2016	−2.24	−9.69	15/03/2016	−2.38	−10.30	0.06	0.37	1.49	0.93
MUACHEMA TRIB	11/06/2016	−0.70	1.41	–	–	–	−0.35	0.42	1.65	0.52
S1-3KD06	15/06/2016	−2.69	−9.45	09/03/2016	−2.78	−10.77	−2.87	0.15	1.31	0.41
GD31	15/06/2016	−3.36	−13.36	09/03/2016	−3.45	−13.72	−0.61	0.53	2.65	0.47
MUK DAM	15/06/2016	−0.07	2.66	09/03/2016	0.30	5.72	−1.68	0.04	1.32	0.59
MUK DWS	15/06/2016	−1.12	−1.15	09/03/2016	−0.86	1.14	−1.66	0.13	1.35	0.51
KINGOMBERO	25/06/2016	−3.03	−11.29	11/03/2016	−3.06	−11.46	−4.17	0.30	–	0.35
Z1-122	10/06/2016	−2.25	−6.65	04/03/2016	−2.18	−5.83	−1.80	0.26	1.01	0.82
Z1-125	10/06/2016	−2.70	−9.39	04/03/2016	−2.73	−10.24	−4.09	0.37	1.48	0.26
Z1-124	10/06/2016	−2.61	−9.37	04/03/2016	−2.87	−9.12	−0.86	0.28	1.42	0.87
D/16/10	10/06/2016	−1.40	−2.81	04/03/2016	−1.30	−2.39	−0.36	0.10	1.45	1.07
Z1-121B	10/06/2016	−3.10	−12.13	05/03/2016	−2.92	−11.47	−0.18	0.54	0.68	0.96
Z1-116	15/06/2016	−3.02	−12.04	11/03/2016	−2.83	−11.69	−0.11	0.21	1.12	1.13
C/07/09	10/06/2016	−2.55	−9.71	11/03/2016	−2.40	−9.58	−0.19	0.11	0.51	1.26
A/01/11	14/06/2016	−2.71	−9.67	05/03/2016	−2.49	−8.93	−0.08	0.11	1.31	1.18
Z2-103	11/06/2016	−2.69	−9.74	05/03/2016	−2.79	−10.35	0.16	0.03	1.40	0.80
D/203/27	14/06/2016	−2.70	−9.26	08/03/2016	−2.64	−9.71	−0.22	0.32	0.39	1.07
DB/MS/LST	13/06/2016	−2.88	−10.71	05/03/2016	−2.82	−10.20	−0.05	0.20	0.98	0.88
Z1-135	08/06/2016	−1.97	−6.63	02/03/2016	−2.15	−7.47	−0.58	0.01	2.45	0.76
Z2-112	08/06/2016	−2.40	−7.71	03/03/2016	−2.45	−8.44	−2.80	0.03	1.25	0.55
Z1-140	15/06/2016	−3.12	−12.26	09/03/2016	−3.11	−12.14	−0.41	0.30	2.02	0.96
Z2-104	16/06/2016	−2.64	−9.35	03/03/2016	−2.56	−9.59	−0.19	0.29	2.05	1.04
Z1-110	16/06/2016	−2.18	−5.85	03/03/2016	−1.90	−4.86	−0.73	−0.09	1.36	1.00
DB/FI/HP	16/06/2016	−3.07	−12.39	03/03/2016	−2.96	−11.37	−0.19	0.33	1.54	0.49
Z3-96	11/06/2016	−2.58	−9.70	08/03/2016	−2.55	−8.64	−0.02	0.14	0.75	1.33
E/29/01	11/06/2016	−2.66	−8.83	08/03/2016	−2.55	−8.78	−0.08	−0.10	0.60	1.10
A/09/11	14/06/2016	−1.86	−5.61	08/03/2016	−1.68	−5.03	−0.01	0.07	0.81	1.24
MIVUMONI	15/06/2016	−3.06	−11.60	09/03/2016	−3.02	−12.12	−3.39	0.62	2.47	0.14
C/15/10	09/06/2016	−3.15	−11.56	09/03/2016	−2.97	−11.72	−1.33	0.45	4.02	0.33
C/109/21	15/06/2016	−3.16	−13.07	09/03/2016	no data	no data	−0.66	0.52	3.63	0.47
C/12/12	09/06/2016	−2.97	−12.71	10/03/2016	−2.93	−12.47	−1.25	0.67	1.12	0.50
C/06/12	09/06/2016	−3.10	−12.40	10/03/2016	−3.20	−9.94	−3.11	0.58	1.85	0.15
C/19/10	09/06/2016	−2.71	−11.00	10/03/2016	−3.04	−10.20	−4.41	0.06	1.59	0.33
D/129/19	06/06/2016	−3.03	−13.27	01/03/2016	−3.08	−13.27	−3.45	0.48	2.77	0.11
DB/MH/CO	07/06/2016	−2.79	−11.82	02/03/2016	−2.75	−11.77	0.04	0.40	1.83	0.72
Z1-141	13/06/2016	−2.06	−7.02	13/03/2016	−2.05	−7.34	0.04	−0.38	0.75	2.38
UK-WL	11/06/2016	−3.04	−13.27	06/03/2016	−2.99	−12.77	−0.12	0.32	0.85	1.21
D/103/16	06/06/2016	−3.20	−14.18	08/03/2016	−3.16	−13.74	−0.08	0.46	1.66	0.78
LUKORE-SEC. SCHOOL	09/06/2016	−3.00	−11.74	10/03/2016	−3.06	−11.77	−0.14	0.54	1.00	0.56

Table 3 (*continued*)

Code	Data	$\delta^{18}O$	$\delta^{2}H$	Data	$\delta^{18}O$	$\delta^{2}H$	SI calcite	SI quartz	Na/Cl	Ca/HCO_3
Z1-118	10/06/2016	−2.75	−10.36	11/03/2016	−2.89	−10.57	−0.31	0.32	1.50	1.13
VIN-WL	13/06/2016	−2.85	−11.61	11/03/2016	−3.27	−8.99	−0.04	0.13	0.69	1.06
BASE_BH_3	17/06/2016	−3.25	−12.93	16/03/2016	−3.20	−13.12	−0.24	0.47	1.27	1.22
BASE_BH_7	17/06/2016	−3.14	−12.39	16/03/2016	−3.23	−12.70	−0.90	0.63	3.55	0.55
DB/KI/ST	18/06/2016	−3.29	−12.84	16/03/2016	−3.34	−11.15	−1.13	0.54	2.67	0.28
Z3-102B	16/06/2016	−2.40	−8.88	–	–	–	0.04	−0.02	1.23	0.95
BH302	23/06/2016	−2.88	−9.89	–	–	–	−1.76	0.42	2.05	0.55
DIANI	22/06/2016	−0.29	1.19	–	–	–	−0.30	−0.34	0.70	5.77
MSW BEACH	22/06/2016	−2.28	−7.34	–	–	–	−0.03	0.18	0.73	1.30
KIS_21	23/06/2016	−2.62	−8.27	–	–	–	−2.21	0.22	1.61	0.72
KIS_65	23/06/2016	–	–	–	–	–	−2.84	0.35	2.11	0.66
GD14_5	17/06/2016	−2.78	−10.72	–	–	–	−0.14	−0.14	0.54	2.70
GD14_ 35	17/06/2016	−2.90	−10.95	–	–	–	0.36	−0.02	0.81	0.90
C/05/09	24/06/2016	−3.03	−10.62	–	–	–	0.20	0.07	1.26	0.91
C/03/09	24/06/2016	−2.81	−9.69				0.05	−0.04	0.77	1.06

Up to the Shimba Hills, it is possible to distinguish two types of processes affecting deep wells located and screened only in the Mazeras sandstone (Fig. 9). The samples of group 'D' located in this geological formation present high silica concentration and are saturated with respect to quartz. Based on the Ca-HCO_3 and Na-Cl relationships the samples are enriched in HCO_3 and Na, resulting from silicate weathering, mainly-feldspar (Appelo and Postma, 2005). For this reason, these samples are unsaturated with respect to calcite (Table 3).

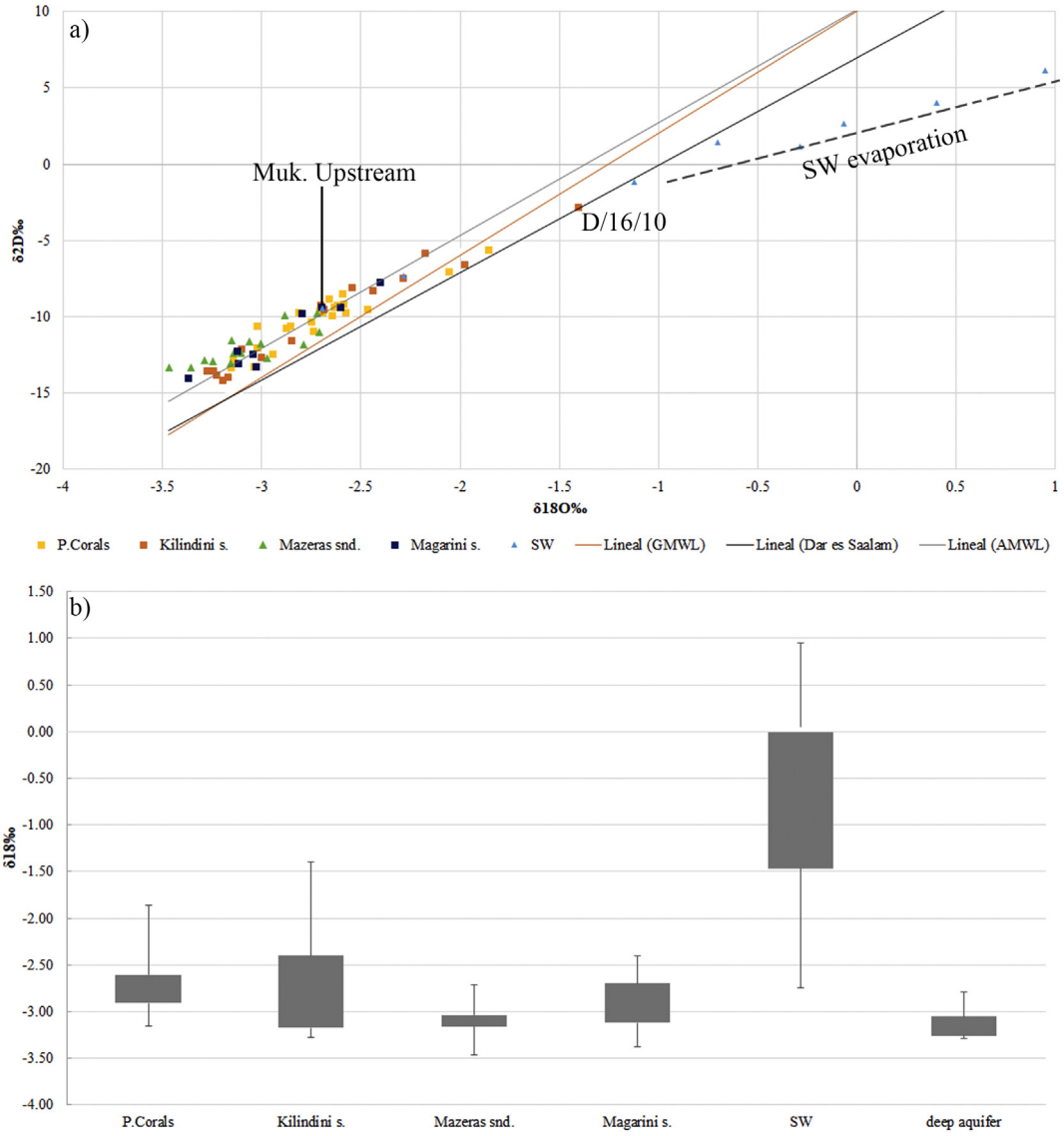

Fig. 11. a) $\delta^{18}O$ vs. $\delta^{2}H$ (δD) of water samples and the Global Meteoric Water Line (GMWL) $\delta^{2}H = 8 * \delta^{18}O + 10‰$ (orange line), Dar es Salaam local meteoric water line $\delta^{2}H = 7.05 * \delta^{18}O + 7‰$ (black line) and African Meteoric Water Line (AMWL) $\delta^{2}H = 7.4 * \delta^{18}O + 10.1‰$ (grey line). The dotted line refers to surface water evaporation; b) Box plot that shows the maximum, minimum and median of $\delta^{18}O$ for each geological formation.

The EC range of these samples is between 260 and 313 μS/cm. However, the rest of the samples in Mazeras sandstone formation, north of the mining site are of the hydrochemical group 'C'. These samples, compared to group 'D', have lower silica concentration but despite this, they are also unsaturated with respect to calcite, and the saturation index is less negative than in group 'D' (Table 2). Silicate weathering in this facies is less significant compared to that in group 'D', even though they are more enriched in Na (Fig. 10c) and present higher values of EC (from 499 to 666 μS/cm). This may be due to increased evapotranspiration.

Li concentration is used as a tracer of flow dynamics of the aquifer (Folch et al., 2011). In the study area, the same ratio of Na/Li (2–5) in the deep aquifer samples and the samples of the group 'C and D' seems to indicate that recharge of the deep aquifer originates in the Shimba Hills range (Fig. 10b).

The hydraulic continuity of Shimba Hills aquifer and the Mazeras Fm. deep aquifer is also confirmed by the water isotopic data since the composition of most samples of the deep aquifer is in the same isotopic interval as the samples from Shimba Hills (Fig. 11a). Some samples located in the deep aquifer in zone 2 have the same hydrochemical facies (group 'C') as the samples located in the Shimba Hills. These samples are from some Base Titanium boreholes screened in Jurassic materials (Kambe, Mtomkuu and Sandstones Fm.). In addition, the EC values of these samples are in the same range (370 μS/cm) as results from the samples of group 'C'. This suggests hydraulic continuity along the Mazeras sandstone, which is also confirmed by seasonal changes in deep groundwater level (Fig. 7). The time lag between a rainfall event and the groundwater level indicates hydraulic connection throughout the Mazeras Fm. and the recharge area of the deep aquifer. This is also confirmed by artesian (flowing) behaviour during the drilling of some of Base Titanium's wells that are only screened in the deep aquifer.

The redox values (Eh from +94 to +191 mV) and dissolved oxygen (DO from 0.8 to 4 mg/L) found in the Base Titanium boreholes tapping the deep aquifer are higher than those of the samples of group 'D' located in the Shimba Hills, and show that there is no significant inflow of shallow groundwater induced by the abstractions since, the Eh and DO values would be higher. This points to semi-confined conditions suggesting the presence of a semi-confining layer (data not shown) (Fig. 12). Indeed, the artesian flow in two Base Titanium boreholes indicates the presence of this confining and/or semi-confining layer (Fig. 2). The permeability of this aquitard varies across the study area depending on geological formation and is affected by the paleochannels that present higher permeability and, also by some deep wells with screens in both the shallow and deep aquifer. The presence of a semi-confining layer dividing a formation into two aquifer units has been observed elsewhere (Manzano et al., 2013). The identification of this layer and detailed characterization of the groundwater system modifies the former conceptual model of a single coastal aquifer into a more complex but still hydrogeologically simple system consisting of two separate layers with an aquitard in between. Other deep well samples present facies typical of group 'A', due to the screened sections of these boreholes being in multiple geological materials, taking water from Pleistocene corals, Kambe limestone, Mtomkuu Fm., and probably Mazeras Fm. as well. These wells show higher values of EC (590 μS/cm) and higher pH values (6.9 and 7.2 respectively) than the wells screened only in the Mazeras sandstone. Some KISCOL wells also screened in both shallow and deep geological formations show hydrochemical facies of group 'A' and a similar range of EC and pH.

The KISCOL boreholes (BH302 and BH310) located in the sugar fields in zone 1 have a heavier isotopic composition than boreholes screened only in the deep aquifer, and also different hydrochemical composition. This isotopic range would appear to be due to the multiple screened intervals in the KISCOL wells, presumably aimed at maximizing groundwater abstraction by capturing water from different aquifer units. Water from both boreholes show silicate weathering, but while BH310 has a Ca-HCO_3 facies with $\delta^{18}O = -2.72‰$, borehole BH302 presents a Na-Ca-HCO_3 facies with lighter water isotopic composition ($\delta^{18}O = -2.88‰$). Considering that the average error for $\delta^{18}O$ is ±0.05, the two samples appear to be slightly different suggesting that BH310 has a greater proportion of water from the shallow aquifer which has heavier isotopic composition compared to BH302. This supposition is backed up by a comparison of Na/Li ratio (Fig. 10b), as BH302 with a hydrochemical facies typical of the deep aquifer has lower Na/Li ratio (2.5–1.5) than BH310 (>3.0) with hydrochemical facies typical of the shallow aquifer. In addition, the BH310 $\delta^{18}O$ change from March (−2.94‰) to June (−2.72‰) may indicate that during the dry season a higher proportion of the groundwater being abstracted is from the deep aquifer. Moreover, the facies of this point changes from Ca-Na-HCO_3 in March, incorporating Na from the deep aquifer to Ca-HCO_3 in June, which points to recharge from the shallow aquifer.

Regarding the shallow aquifer formations, the hydrochemical signal of group 'E', all points located in Magarini sands, indicate that this

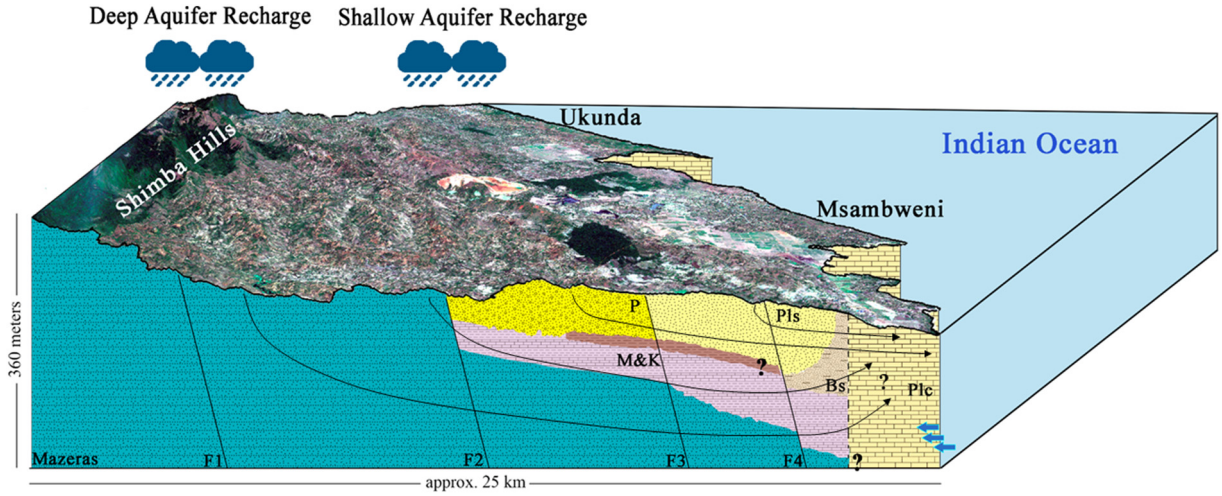

Fig. 12. Schematic conceptual model of the aquifer. The flow lines indicate flow direction and connectivity through the geological formations from the recharge areas for the shallow and deep aquifer. The question marks indicate the existence of a clay layer, the connectivity between the Mazeras Fm. and Pleistocene corals and the discharge of the deep aquifer. Mazeras (Mazeras Fm.), M&K (Mtonkuu and Kambe Fm.), P (Magarini sands), Pls (Kilindini sands), Bs (bioclastic sands with clay lenses), Plc (Pleistocene corals), and in brown color the clay layer acting as an intercalated aquitard. F1 to F4 indicates the main fault in the study area. (For interpretation of the references to color in this figure legend, the reader is referred to the web version of this article.)

geological formation acts as the recharge area for the shallow groundwater system. Low pH (average of 5.6) and EC (between 50 and 170 μS/cm) compared with the samples located in other geological formations indicate the absence of soluble carbonate minerals and suggest less interaction with the soil and the unsaturated zone (Table 2).

The different composition of the samples located in the Mazeras sandstone and in the Magarini sands, with lower salinity and Cl and higher Si concentrations in samples from the second geological formation point out that there is no hydraulic connection between these two geological formations. However, the groundwater contour map (Fig. 5) indicates the possibility of deep groundwater flow from the Shimba Hills to the sea. These two factors indicate that the fault located East of the Shimba Hills (Fault 2 of Fig. 2) acts as a low permeability boundary, forcing recharge from the Shimba Hills to the deep aquifer located under the shallow geological formations (Magarini sands, Pleistocene sands and corals).

Groundwater flowing through the shallow groundwater system becomes enriched in Ca and HCO_3 (Group 'A' samples), due to the geology (carbonate, mainly limestone - Pleistocene materials) of the southern area. The modified Stiff diagrams show how this enrichment in Ca and HCO_3 going from inland (Magarini sands) toward the coast point to connection through the geological formation. The relatively high Si concentration in Pleistocene formations and in samples taken from an upwelling/spring located on the tidal Msambweni beach in zone 1 (over 10 mg/L Si) confirms the connection between all the shallow aquifer systems (Magarini sands, Kilindini sands and Pleistocene corals) (Table 2). On the other hand, samples with low Si concentration located in zone 1 and 2 along the Pleistocene materials indicate a possible dilution of Si concentration due to local recharge through these geological formations. Indeed, the wells located along the coast which are not affected by saline intrusion show a slight EC decrease during rainy periods, indicating shallow local recharge in the Pleistocene corals. Some samples near the south coast present lighter isotopic composition, more similar to the samples from the deep aquifer. This further confirms the connectivity between diverse geological materials in the paleochannel areas due to the process of erosion and deposition during the original formation of the channels.

Furthermore, considering the change in isotopic composition across the field surveys, the samples showing the greater percentage change in water isotopic composition when comparing March and June field surveys are the samples with Na-Cl facies (group 'B'). This is due to the isotopic mixing produced by seawater intrusion. Seawater intrusion is also confirmed by the high Na/Li ratio (13–65) (Fontes and Matray, 1993) following the mixing seawater line (Line 1 Fig. 10b). However, samples from the shallow aquifer located in Magarini sands with Na-HCO_3-Cl facies (group 'E') also present higher isotopic change between seasons due to the influence of local rainfall during the wet season. On the contrary, samples in the deep aquifer (group 'D') present little isotope variation (Fig. 11b), suggesting a uniform and constant recharge in the deep aquifer throughout the seasons. Samples located in the Magarini sands and the Mazeras sandstone (group 'E' and 'D' respectively) present low values but a high variation of EC between seasons providing further evidence of their role as recharge areas.

There is a negative correlation ($P < 0.01$) between Si concentration and water isotope composition ($\delta^{18}O$), except for in surface water samples and those allowing evaporation from a free surface (Fig. 10d). This confirms the main recharge areas previously mentioned: the Mazeras sandstone and Magarini sands, and the two main flow paths: one from the Mazeras sandstone to the deep aquifer and a second from the Magarini sands to the coral limestone. The change in isotopic composition and Si concentration (among others) along the flow path of the shallow aquifer formation shows that besides the Magarini sands, significant recharge of the shallow aquifer is also occurring on the Pleistocene formations. Finally, the fact that significant DO concentrations were measured in many wells (Table 2) indicates that dissolved oxygen, pH and Eh are not in chemical equilibrium. This observation may suggest that the water under more reducing conditions coming from the Magarini sands mixes with more oxygenated water from recharge through the Pleistocene materials as the shallow aquifer is recharged across the study area. That said, DO values in zone 4, which range from 3.1 to 5.7 mg/L, are lower, suggesting other processes may be taking place in this area (Table 2).

Seasonal variation in groundwater level in wells in zone 4, along with lower DO values and the isotopic composition of samples from this area may indicate the existence of a clay layer associated with the marine sediments of the Kambe and Mtomkuu Fm. The low permeability of this layer would limit local recharge to the deep aquifer in the lower part of the basin, explaining the relatively lighter isotopic composition of groundwater recharged in the higher areas. This explanation is in agreement with observed groundwater level variation after extreme rainfall events in which the limited change in groundwater level after rainfall indicates the absence of direct recharge (Fig. 6b).

Regarding surface water-groundwater interaction, although it cannot be defined along all rivers with the potentiometric data (Fig. 5), the hydrochemical results indicate that the slightly brackish Ramisi River is being fed by the aquifer as the point sampled downstream has lower salinity than the sample from upstream (Fig. 9), which can be explained by dilution as lower salinity groundwater flows into the river. The Li concentration in the samples from Ramisi River comes from the hot springs at Mwananyamala (Tole, 1990) (Line 2 Fig. 10b). The potentiometric map shows that the Mukurumudzi river is also effluent (gaining), which agrees with the composition of point S1-3KD06 ($\delta^{18}O = -2.6‰$) being in the same range as groundwater. However, river-aquifer interactions are difficult to ascertain with this kind of data as the sampling points may be affected by water released at dams and subject to other hydrochemical processes.

6.2. Effects of La Niña drought on the groundwater system and its hydrochemistry

There is insufficient groundwater level data to evaluate the effect of La Niña in the shallow aquifer as data in most points starts in 2016. However, during the La Niña event, the wells located on the Kilindini sands (except in zone 4) and Magarini sands had higher groundwater drawdown (3.4 to 1.4 m) compared to the wells located on Pleistocene corals. In the deep aquifer, with data available since 2012 in the Zone 2, it is possible to observe a larger recession in groundwater level during the La Niña event compared to that seen in 2012, possibly caused by increased abstraction rates during the drought period.

The behaviour of the system in 2014 is the one expected for an area affected by the monsoon in a tropical area (Isa et al., 2014). The recharge volume difference in 2014 between seasons produces a hydrochemical differentiation of the composition of the samples. During the post-monsoon (wet season-June 2014) inland samples display an elevated concentration of mineral ions (Ca and Mg). This increment during the wet season could be explained by the associated reversible cation exchange. Oppositely, during La Niña event, there are not fresh water salinity differences between campaigns in 2016 due to the low recharge caused by the low rainfall in the wet season. Zone 4 is an exception to this pattern, as there is no hydrochemical variation between field surveys in 2014 and 2016 confirming the existence of a clay layer in this area, associated with the marine sediments of the Kambe and Mtomkuu Fm.

In the coastal area, during the pre-monsoon (dry season-March 2014) there is a higher concentration of Na and Cl due to an increase of seawater intrusion caused by lower recharge responsible to modify the balance between fresh and saline water. As expected, samples affected by saline intrusion shows higher salinity during the dry season due to lower recharge. The EC values during the dry season are around 22% on average higher than the wet season. On the contrary, during La Niña, this increment on saline intrusion on the coastal samples during the dry season is lees compared to 2014. The increment on CE values

during the dry season is only 12% on average compared to the wet season. Therefore, during La Niña drought the whole year behaves as a "dry season" causing its main impact in the coastal area.

7. Limitations of the groundwater conceptual model and implications

In this study, a groundwater conceptual model of the Kwale aquifer has been defined and the effects of La Niña on the hydrodynamics of the system have been assessed. However, it should be noted that the research here presented has some limitations and uncertainties.

One important limitation is that the effect of "La Niña" in 2016 on the shallow aquifer is based only on groundwater level data from the same year, which limits the understanding of the effect of this drought on the shallow aquifer system. Moreover, the hydrodynamics of the shallow aquifer in some areas are not yet completely understood. Wells located in zone 4 did not seem to be affected by the La Niña event. However, the behaviour of the system under longer drought periods is unknown. In the same way, hydrochemical and isotopic data from wells located in the Kilindini sands in zone 2 indicate different aquifer hydrodynamics in this area.

Another important issue is incomplete knowledge of the full extent of the aquitard that separates the groundwater system into the shallow and deep aquifer levels. While this layer is clearly identified in Zone 2 in the area of Base Titanium boreholes, its presence or absence in zones 1, 3 and 4 not affected by the paleochannels is unknown due to the lack of deep boreholes in those areas. Potential connectivity between the aquifer units must be taken into account in terms of groundwater exploitation since intense abstraction in the deep aquifer could affect the shallow aquifer levels. The connectivity between the shallow and deep aquifer levels in the Pleistocene corals is also not well understood. While it is thought that the Pleistocene corals overlay the Mazeras Fm. in depth near the coast, there is a lack of knowledge about how the deep aquifer connects with the sea and thus the potential for salinization of both aquifer levels.

It was possible to identify two paleochannels located in zone 1 and 3. However, the full extent and continuity of these sedimentary layers are not completely understood, which in turn limits understanding of the hydraulic properties of the formation and the potential hydraulic connectivity with surrounding formations. In addition, the exact borders of the paleochannels and their connectivity with the sea are undetermined. Therefore, although water level and quality in the area of the paleochannels did not appear to be affected by La Niña 2016, the behaviour of the system under longer drought periods and the effect of the paleochannels at a regional scale cannot be defined. For example, in a prolonged drought it is possible that the paleochannels could act as preferential zones of saline intrusion.

The hydrochemical data from the Ramisi River suggests that the aquifer feeds water into the middle reaches of the river. However, the river-aquifer relation along the river length and the effect of the drought period in the river is not fully understood due to the lack of groundwater data from areas bordering the stream.

The drought that occurred in 2016 did not have dramatic effects on water level. However, due to the above-mentioned limitations and uncertainties, the consequences of a future longer drought period cannot be reliably predicted.

8. Summary and conclusions

Drought provoked by La Niña and IOD conditions harassed the Greater Horn of Africa region in 2016. One of the affected areas was the coastal county of Kwale (Kenya), a rural area, where the effects of drought on the aquifer system can be used as an indication of likely effects throughout the coastal strip sharing similar geology.

Before analysing the effect of the La Niña 2016 event on the groundwater system, a conceptual model of the hydrogeological system was defined. By means of a geophysical approach, it was possible to define the aquifer geometry and its limits. The studied aquifer system is formed by two hydrogeological systems: one shallow aquifer composed of younger geological materials (Pliocene and Pleistocene formations) and a deep aquifer composed of older materials (Jurassic and Triassic) which outcrops inlandwards, in the Shimba Hills Range. In the middle part of the area, the deep aquifer acts as a confined aquifer due to the presence of an aquitard with very low permeability located between the younger and the older materials. However, the confined behaviour of the deep aquifer changes along the study area, becoming less confined and so, the connectivity between the shallow and deep aquifer increases. This is due to the presence of paleochannels, one in the northern area (zone 3) and another in the southern area (zone 1). The shallow unconfined aquifer is recharged directly by local rainfall across the area, except in the lower part of zone 4, where the shallow aquifer behaves as semiconfined/confined due to the heterogeneity of geological materials and the presence of clay/low permeability materials. The deep aquifer is recharged in the Shimba Hills area by preferential flow though faults and joints. The discharge of both hydrogeological systems is along the littoral to the Indian Ocean, through abstraction by the different water users of the region (communities, agriculture, mining and tourism) and through direct evaporation and evapotranspiration, etc.

One of the effects of the La Niña drought of 2016/2017 was the reduction in the recharge during this event. In 2016 recharge was reduced by 78% compared to the wet year of 2014 and reduced by 69% compared to a year with normal annual rainfall (2013). In effect, the wet season of 2016 behaved like a continuation of the dry season.

The change in recharge caused by the La Niña drought meant that groundwater quality remained constant in the samples located inland throughout the year, compared to the seasonal differences observed in 2014. On the other hand, due to a reduction in recharge attributed to the La Niña drought, salinity in the coastal wells increased between March and June instead of being reduced, as occurs in normal years.

Regarding groundwater quality beyond the coast, results seem to indicate that nitrate pollution is not a current significant problem in the study area, and what exists is mainly linked to urban areas.

The effect of the La Niña 2016/17 event on the aquifer system in Kwale County has important implications for groundwater management, as the "recovery" of groundwater levels and quality is damaged in the absence of normal wet season rainfall. Effectively, this region experienced an extended dry season from the end of 2015 to the middle of 2017, with a consequent decrease in aquifer water levels and an increase in saline intrusion. For successful long-term management of water resources, the effects of long drought periods must be considered together with impacts associated with increased groundwater demand throughout Africa. Intensification of agriculture, industrialization and population growth along with the effects of extended droughts may act in damaging synergy on Africa's groundwater systems.

Acknowledgments

The authors gratefully acknowledge the support of Kenya's Water Resource Authority (formerly WRA), the Kwale Country Government, Base Titanium Ltd., Kwale International Sugar Company Ltd. and Rural Focus Ltd. This research was funded by the UK Government via NERC, ESRC and DFID as part of the Gro for GooD project (UPGro Consortium Grant: NE/M008894/1). We appreciate the constructive comments and English review done by Nancy Gladstone.

Appendix A. Supplementary data

Supplementary data to this article can be found online at https://doi.org/10.1016/j.scitotenv.2019.01.198.

References

Anglés, M., Folch, A., Oms, O., Maestro, E., Mas-Pla, J., 2017. Stratigraphic and structural controls on groundwater flow in an outcropping fossil fan delta: the case of Sant Llorenç del Munt range (NE Spain). Hydrogeol. J. 25, 2467–2487.

Appelo, C.A.J., Postma, D., 2005. Geochemistry, Groundwater and Pollution. A.A. Balkema Publishers.

Armengol, S., Manzano, M., Bea, S.A., Martínez, S., 2017. Identifying and quantifying geochemical and mixing processes in the Matanza-Riachuelo Aquifer System, Argentina. Sci. Total Environ. 599–600, 1417–1432.

Bakari, S.S., Aagaard, P., Vogt, R.D., Ruden, F., Brennwald, M.S., Johansen, I., Gulliksen, S., 2012. Groundwater residence time and paleorecharge conditions in the deep confined aquifers of the coastal watershed, South-East Tanzania. J. Hydrol. 466–467, 127–140.

Baudoin, M.A., Vogel, C., Nortje, K., Naik, M., 2017. Living with drought in South Africa: lessons learnt from the recent El Niño drought period. Int. J. Disaster Risk Reduct. 23, 128–137.

Behera, S.K., Luo, J.J., Masson, S., Delecluse, P., Gualdi, S., Navarra, A., Yamagata, T., 2005. Paramount impact of the Indian Ocean dipole on the east African short rains: a CGCM study. J. Clim. 18, 4514–4530.

Buckley, B.S., 1981. Report on a Visit to Assess Groundwater Potential of the Kenya Coast of Malindi (Including Proposals for the South Coast Groundwater Resources Project). Institute of Geological Sciences (IGS), Wallingford, UK.

Cannon, R.T., Simiyu Siambi, W.M.N., Karanja, F.M., 1981. The Proto-Indian Ocean and a probable paleozoic/mesozoic triradial rift system in East Africa. Earth Planet. Sci. Lett. 52, 419–426.

Caswell, P.V., 1953. Geology of the Mombasa-Kwale Area. Geological Survey of Kenya.

Commission on Revenue Allocation, 2011. URL. https://www.crakenya.org/county/kwale.

Commission on Revenue Allocation, 2018. URL. https://www.crakenya.org/county/kwale.

Comte, J.C., Cassidy, R., Obando, J., Robins, N., Ibrahim, K., Melchioly, S., Mjemah, I., Shauri, H., Bourhane, A., Mohamed, I., Noe, C., Mwega, B., Makokha, M., Join, J.L., Banton, O., Davies, J., 2016. Challenges in groundwater resource management in coastal aquifers of East Africa: investigations and lessons learnt in the Comoros Islands, Kenya and Tanzania. J. Hydrol. Reg. Stud. 5, 179–199.

Custodio, E., 2013. Trends in groundwater pollution: loss of groundwater quality & related action. Groundwater Governance: A Global Framework for Country.

Custodio, E., Llamas, M., Samper, J., 1997. La evaluación de la recarga a los acuíferos en la planificación hidrológica. International Association of Hydrogeologists-Spanish Group, Madrid.

CWSB, 2013a. Coastal Water Services Board-Water Point Mapping Report: Kwale County. URL. www.cwsb.go.ke.

CWSB, 2013b. Coastal Water Services Board - Strategic Plan (2013–2017). URL. www.cwsb.go.ke.

Day, J.A., 1993. The major ion chemistry of some southern African saline systems. Hydrobiologia 267, 37–59.

Demlie, M., Titus, R., 2015. Hydrogeological and hydrochemical characteristics of the natal group sanstone, South Africa. S. Afr. J. Geol. 118, 33–44.

DiGregorio, A., 2002. Multipurpose Landcover Database for Kenya – Africover. URL. FAOhttp://www.fao.org/geonetwork/srv/en/metadata.show?id=38098&currTab=simple.

Edmunds, W.M., Guendouz, A.H., Mamou, A., Moulla, A., Shand, P., Zouari, K., 2003. Groundwater evolution in the Continental Intercalaire aquifer of southern Algeria and Tunisia: trace element and isotopic indicators. Appl. Geochem. 18, 805–822.

Ezekiel, I.T., Maurice, N., K'orowe, M., 2016. Seawater intrusion vulnerability assessment of a coastal aquifer: north coast of Mombasa, Kenya as a case study. J. Eng. Res. Appl., 2248–9622. www.ijera.com (ISSN 6).

Faulwetter, J.L., Gagnon, V., Sundberg, C., Chazarenc, F., Burr, M.D., Brisson, J., Camper, A.K., Stein, O.R., 2009. Microbial processes influencing performance of treatment wetlands: a review. Ecol. Eng. 35, 987–1004.

Folch, A., Menció, A., Puig, R., Soler, A., Mas-Pla, J., 2011. Groundwater development effects on different scale hydrogeological systems using head, hydrochemical and isotopic data and implications for water resources management: the Selva basin (NE Spain). J. Hydrol. 403, 83–102.

Fontes, J., Matray, J., 1993. Geochemistry and origin of formation brines associated with triassic salts. Chem. Geol. 109, 149–175.

Foster, T., Hope, R., 2016. A multi-decadal and social-ecological systems analysis of community waterpoint payment behaviours in rural Kenya. J. Rural. Stud. 47, 85–96.

Hargreaves, G., Samani, Z., 1982. Estimating potential evapotranspiration. J. Irrig. Drain. Div. - ASCE 108, 225–230.

Isa, N.M., Aris, A.Z., Sulaiman, W.N.A.W., Lim, A.P., Looi, L.J., 2014. Comparison of monsoon variations over groundwater hydrochemistry changes in small Tropical Island and its repercussion on quality. Hydrol. Earth Syst. Sci. Discuss. 11, 6405–6440.

Kelbe, B.E., Grundling, A.T., Price, J.S., 2016. Modelling water-table depth in a primary aquifer to identify potential wetland hydrogeomorphic settings on the northern Maputaland Coastal Plain, KwaZulu-Natal, South Africa. Hydrogeol. J. 24, 249–265.

Kempen, B., 2007. Soil and Terrain Database for Kenya (ver.2) (KENSOTER).

Levin, N.E., Zipser, E.J., Ceding, T.E., 2009. Isotopic composition of waters from Ethiopia and Kenya: insights into moisture sources for eastern Africa. J. Geophys. Res. Atmos. 114, 1–13.

MacDonald, A.M., Calow, R.C., MacDonald, D.M.J., Darling, W.G., Dochartaigh, B.E.O., 2009. What impact will climate change have on rural groundwater supplies in Africa? Hydrol. Sci. J. 54, 690–703.

Manzano, M., Custodio, E., Higueras, H., 2007. Groundwater and its functioning at the Doñana RAMSAR site wetlands (SW Spain): role of environmental isotopes to define the flow system. Advances in Isotope Hydrology and Its Role in Sustainable Water Resources Management. IHS–2007, Proc. Symp. Viena. International Atomic Energy Agency, Wien, pp. 149–160.

Manzano, M., Custodio, E., Lozano, E., Higueras, H., 2013. Relationships between wetlands and the Doñana coastal aquifer (SW Spain). In: Taylor & Francis (Ed.), Groundwater and Ecosystems, pp. 169–182.

Mckenzie, J.M., Mark, B.G., Thompson, L.G., Schotterer, U., Lin, P.-N., 2010. A hydrogeochemical survey of Kilimanjaro (Tanzania): implications for water sources and ages. Hydrogeol. J. 18, 985–995.

Menció, A., Folch, A., Mas-Pla, J., 2012. Identifying key parameters to differentiate groundwater flow systems using multifactorial analysis. J. Hydrol. 472–473, 301–313.

Menció, A., Mas-Pla, J., Otero, N., Regàs, O., Boy-Roura, M., Puig, R., Bach, J., Domènech, C., Zamorano, M., Brusi, D., Folch, A., 2016. Nitrate pollution of groundwater; all right…, but nothing else? Sci. Total Environ. 539, 241–251.

Miller, S., 1994. Handbook for Agrohydrology. Natural Resources Institute.

Mpelasoka, F., Awange, J.L., Zerihun, A., 2017. Influence of coupled ocean-atmosphere phenomena on the Greater Horn of Africa droughts and their implications. Sci. Total Environ. 610611, 691–702.

Mtoni, Y., Mjemah, I.C., Bakundukize, C., Van Camp, M., Martens, K., Walraevens, K., 2013. Saltwater intrusion and nitrate pollution in the coastal aquifer of Dar es Salaam, Tanzania. Environ. Earth Sci. 70, 1091–1111.

Mumma, A., Lane, M., Kairu, E., Tuinhof, A., Hirji, R., 2011. Kenya groundwater governance case study. URL. https://openknowledge.worldbank.org/handle/10986/17227, Accessed date: 11 May 2017 (WWW Document).

Mutemi, J., 2003. Climate Anomalies Over Eastern Africa Associated With Various ENSO Evolution Phases. University of Nairobi, Kenya.

Ndlovu, M., Demlie, M., 2016. Hydrogeological characterization of the Kosi Bay Lakes system, north-eastern South Africa. Environ. Earth Sci. 75, 1334.

Neumann, B., Vafeidis, A., Zimmermann, J., Nicholls, R., 2015. Future coastal population growth and exposure to sea-level rise and coastal flooding - a global assessment. PLoS One 10 (3).

Obura, D.O., 2001. The coastal and marine environment. Mar. Pollut. Bull. 42, 1264–1278.

Ogwang, B.A., Ongoma, V., Xing, Li, Ogou, K.F., 2015. Influence of Mascarene high and Indian Ocean dipole on East African extreme weather events. Geogr. Pannonica 19, 64–72.

Okello, C., Antonellini, M., Greggio, N., Wambiji, N., 2015. Freshwater Resource Characterization and Vulnerability to Climate Change of the Shela Aquifer in Lamu, Kenya. pp. 3801–3817.

Ouedraogo, I., Vanclooster, M., 2016. A meta-analysis of groundwater contamination by nitrates at the African scale. Hydrol. Earth Syst. Sci. Discuss. 1–43.

Rais-Assa, R., 1988. Stratigraphy and geodynamics of the Mombasa Basin (Kenya) in relation to the genesis of the proto-Indian Ocean. Geol. Mag. 125, 141–147.

Richey, A.S., Thomas, B.F., Lo, M.-H., Famiglietti, J.S., Swenson, S., Rodell, M., 2015a. Uncertainty in global groundwater storage estimates in a total groundwater stress framework. Water Resour. Res. 51, 5198–5216.

Richey, A.S., Thomas, B.F., Lo, M.-H., Reager, J.T., Famiglietti, J.S., Voss, K., Swenson, S., Rodell, M., 2015b. Quantifying renewable groundwater stress with GRACE. Water Resour. Res. 51, 5217–5238.

Sappa, G., Ergul, S., Ferranti, F., Sweya, L.N., Luciani, G., 2015. Effects of seasonal change and seawater intrusion on water quality for drinking and irrigation purposes, in coastal aquifers of Dar es Salaam, Tanzania. J. Afr. Earth Sci. 105, 64–84.

Steyl, G., Dennis, I., 2010. Review of coastal-area aquifers in Africa. Hydrogeol. J. 18, 217–225.

Taylor, R.G., Todd, M.C., Kongola, L., Maurice, L., Nahozya, E., Sanga, H., MacDonald, A.M., 2012. Evidence of the dependence of groundwater resources on extreme rainfall in East Africa. Nat. Clim. Chang. 3, 374–378.

Tole, M.P., 1990. Chemical geothermometry and resource potential of low enthalpy geothermal systems in Kenya. Geotherm. Resour. Counc. Trans. 14, 187–193.

Uhe, P., Philip, S., Shah, K., Kimutai, J., Otto, F., Van Oldenborgh, G.J., Singh, R., Arrighi, J., Cullen, H., 2017. Climate and Development Knowledge Network and World Weather Attribution Initiative Raising Risk Awareness.

Uhe, P., Philip, S., Kew, S., Shah, K., Kimutai, J., Mwangi, E., van Oldenborgh, G.J., Singh, R., Arrighi, J., Jjemba, E., Cullen, H., Otto, F., 2018. Attributing drivers of the 2016 Kenyan drought. Int. J. Climatol. 38, e554–e568.

Van Camp, M., Chikira Mjemah, I., Al Farrah, N., Walraevens, K., 2013. Modeling approaches and strategies for data-scarce aquifers: example of the Dar es Salaam aquifer in Tanzania. Hydrogeol. J. 21, 341–356.

Wick, K., Heumesser, C., Schmid, E., 2012. Groundwater nitrate contamination: factors and indicators. J. Environ. Manag. 111, 178–186.